Article

Cell Reports

Translaminar Cortical Membrane Potential Synchrony in Behaving Mice

Graphical Abstract

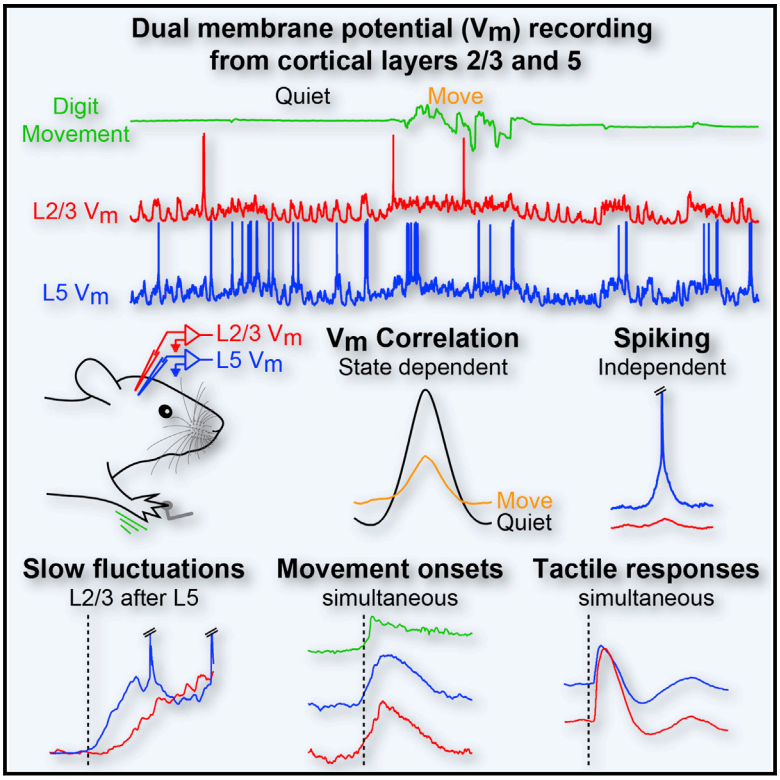

Authors

Wen-Jie Zhao, Jens Kremkow, James F.A. Poulet

Correspondence

james.poulet@mdc-berlin.de

In Brief

Zhao et al. use dual whole-cell recordings from primary somatosensory cortical excitatory neurons in layers 2/3 and 5 in awake mice to identify layer-specific cellular properties and firing rates, and they show that translaminar membrane potential synchrony is dependent both on behavioral state and the source of the synaptic input.

Highlights

- We made dual whole-cell recordings from L2/3 and L5 cortical neurons in behaving mice
- Layer-specific membrane properties determine higher mean firing rates of L5 neurons
- Synchrony of translaminar synaptic activity is determined by the origin of input
- L5 neurons signal spontaneous and sensory-triggered movements

Zhao et al., 2016, Cell Reports *15*, 2387–2399
June 14, 2016
http://dx.doi.org/10.1016/j.celrep.2016.05.026

Cell Reports
Article

OPEN ACCESS
CellPress

Translaminar Cortical Membrane Potential Synchrony in Behaving Mice

Wen-Jie Zhao,[1,2,4] Jens Kremkow,[1,2,3,4] and James F.A. Poulet[1,2,*]
[1]Department of Neuroscience, Max Delbrück Center for Molecular Medicine (MDC), Berlin-Buch, Robert-Rössle-Straße 10, 13092 Berlin, Germany
[2]Cluster of Excellence NeuroCure, Neuroscience Research Center, Charité-Universitätsmedizin Berlin, Charitéplatz 1, 10117 Berlin, Germany
[3]Department of Biology, Institute for Theoretical Biology, Humboldt-Universität zu Berlin, Philippstraße 13, 10115 Berlin, Germany
[4]Co-first author
*Correspondence: james.poulet@mdc-berlin.de
http://dx.doi.org/10.1016/j.celrep.2016.05.026

SUMMARY

The synchronized activity of six layers of cortical neurons is critical for sensory perception and the control of voluntary behavior, but little is known about the synaptic mechanisms of cortical synchrony across layers in behaving animals. We made single and dual whole-cell recordings from the primary somatosensory forepaw cortex in awake mice and show that L2/3 and L5 excitatory neurons have layer-specific intrinsic properties and membrane potential dynamics that shape laminar-specific firing rates and subthreshold synchrony. First, while sensory and movement-evoked synaptic input was tightly correlated across layers, spontaneous action potentials and slow spontaneous subthreshold fluctuations had laminar-specific timing; second, longer duration forepaw movement was associated with a decorrelation of subthreshold activity; third, spontaneous and sensory-evoked forepaw movements were signaled more strongly by L5 than L2/3 neurons. Together, our data suggest that the degree of translaminar synchrony is dependent upon the origin (sensory, spontaneous, and movement) of the synaptic input.

INTRODUCTION

Primary sensory cortex is composed of six layers of interconnected microcircuits. Gain- and loss-of-function experiments have shown laminar-specific effects on local cortical processing (Beltramo et al., 2013; Olsen et al., 2012), but how the layers work together remains unclear. The synchrony of action potential (AP) firing across cortical layers is thought to be a fundamental aspect of translaminar processing and is determined by the strength, sign and timing of the underlying synaptic input. Here, we investigate the synaptic mechanisms of cortical synchrony between excitatory neurons in layers 2/3 and 5 in behaving mice.

Measuring translaminar membrane potential (V_m) synchrony and linking it to sensory processing and behavior require simultaneous V_m recordings from different layers in awake animals. However, the vast majority of V_m recordings of cortical neurons in behaving animals have been made from superficial layers (Bennett et al., 2013; Crochet and Petersen, 2006; Gentet et al., 2010; Polack et al., 2013; Poulet and Petersen, 2008; Poulet et al., 2012; Reimer et al., 2014; Zhou et al., 2014). These studies have shown that internally generated, spontaneous network activity dominates the V_m of cortical neurons across cortical regions and is correlated with the behavioral and arousal state. Large-amplitude, slow fluctuations are highly correlated between neighboring layer 2/3 (L2/3) neurons in resting animals but are abolished during movement, resulting in a desynchronized or "active" cortical state (Harris and Thiele, 2011; Poulet and Petersen, 2008). The active state may result from arousal-related effects associated with movement and has been linked to a modulation in sensory responsiveness (Crochet and Petersen, 2006; Otazu et al., 2009; Pinto et al., 2013; Polack et al., 2013; Reimer et al., 2014; Schneider et al., 2014; Vinck et al., 2015; Zhou et al., 2014), adaptation (Castro-Alamancos, 2004), and even perception itself (Bennett et al., 2013; McGinley et al., 2015).

Few studies have examined the V_m activity of deeper layer cortical neurons in behaving animals (McGinley et al., 2015; Schiemann et al., 2015). Extracellular recordings, however, have shown higher spontaneous and sensory-evoked firing rates in deeper layer neurons (de Kock et al., 2007; O'Connor et al., 2010) and, intriguingly, that sensory-evoked and spontaneous spiking have different temporal structures across layers (Sakata and Harris, 2009).

The rodent forepaw somatosensory system is a relevant and accessible model system to investigate cortical sensory processing during behavior. The forepaw has five digits (Figure 1A) that can be used to grasp and manipulate objects as well as discriminate somatosensory stimuli (Milenkovic et al., 2014). We made whole-cell recordings from primary forepaw somatosensory cortex L2/3 and L5 excitatory neurons in awake mice to compare the synchrony and integration of external (sensory) and internal (movement-evoked and spontaneous) synaptic input. Our data highlight layer-specific membrane properties that underlie differences in AP firing and show that translaminar V_m synchrony is dependent both on the behavioral state and the source of synaptic input.

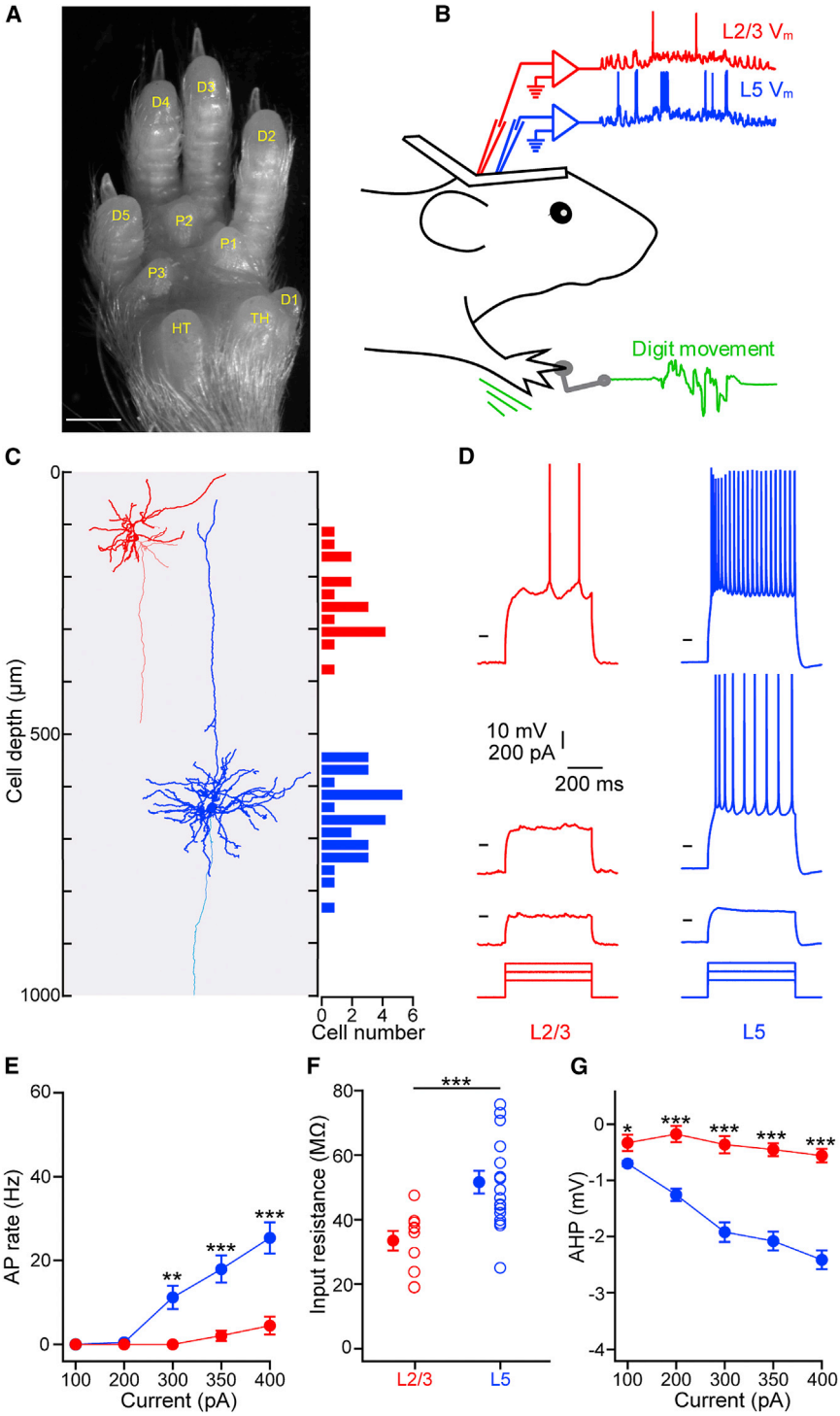

Figure 1. Distinct Membrane Properties of L2/3 and L5 Cortical Pyramidal Neurons

(A) Image of the glabrous skin of the right forepaw showing five digits (D1–D5), three central pads (P1–P3), the thenar pad (TH), and the hypothenar pad (HT) (Waters et al., 1995). Scale bar, 1 mm.

(B) Cartoon schematic showing head-fixed awake mouse with recording electrodes in red (L2/3) and blue (L5), with forepaw digit movement (green) monitored by the sensing arm (gray) that was also used for tactile stimulation.

(C) Biocytin reconstructions of L2/3 (red) and L5 (blue) neurons, with axons in lighter color, next to a histogram showing the depths of all recorded L2/3 and L5 neurons (n = 17 L2/3 neurons and n = 28 L5 neurons) based on micromanipulator reading and biocytin staining.

(D) Three single trial responses of a L2/3 (red) and a L5 (blue) pyramidal neuron to intracellular current injection with different amplitudes (from top to bottom: +400 pA, +300 pA, and +200 pA). The L2/3 example corresponds to the reconstructed L2/3 neuron in (C). Horizontal lines indicate −60 mV for L2/3 and L5.

(E) Plotting the evoked spike rate as a function of current injection amplitude reveals that L5 neurons are more excitable than L2/3 neurons. Filled circles with error bars show mean ± SEM.

(F) L5 neurons have a significantly larger input resistance than L2/3 neurons during hyperpolarizing current injection. Open circles show individual cells.

(G) L5 neurons show a significantly larger amplitude hyperpolarization following positive current injection (afterhyperpolarization [AHP]) than L2/3 neurons at all current amplitudes tested.

For all panels, *p < 0.05, **p < 0.01, and ***p < 0.001.

RESULTS

Distinct Intrinsic Membrane Properties of L2/3 and L5 Primary Somatosensory Forepaw Cortical Excitatory Neurons

To investigate the intrinsic membrane properties of L2/3 and L5 excitatory neurons, we made blind whole-cell patch clamp recordings targeted to the digit 3 cortical representation in primary somatosensory forepaw cortex (S1) in awake mice. Mice were head-restrained and had their right forepaw tethered to the platform (Figure 1B). The tips of the digits 2 and 4 overhung the edge of the platform while the tip of digit 3 was positioned on a flat, circular head of a combined movement sensor and force-feedback tactile stimulating arm. The stimulating arm head was held in contact with the glabrous skin of digit 3 throughout all recordings. Whole-cell recordings from 17 L2/3 neurons were made at subpial depths between 121 and 384 μm (245.30 ± 17.91 μm) and from 28 L5 neurons between 538 and 823 μm (649.43 ± 14.28 μm) (Figure 1C). All neurons had evoked regular-spiking firing patterns during current injection, and a subset (L2/3 = 4/17 and L5 = 15/28 neurons) was confirmed by post hoc biocytin staining to be excitatory pyramidal neurons.

We first examined the intrinsic membrane properties soon after break-in during quiet wakefulness. L5 neurons generated more APs in response to equivalent current injection amplitudes than L2/3 neurons (Figures 1D and 1E). The increased excitability may be due to the higher resting V_m value of L5 neurons during quiet wakefulness ($L2/3_{Mean}$ = −56.92 ± 1.21 mV, n = 12 cells versus $L5_{Mean}$ = –50.70 ± 0.65 mV, n = 19 cells; p < 0.001) and their higher input resistance (Figure 1F; $L2/3_{I/R}$ = 33.46 ± 2.80 MΩ, n = 11 cells versus L5 = 51.66 ± 3.35 MΩ, n = 18 cells; p < 0.001). Interestingly, following the termination of a depolarizing current step, L5 neurons showed a larger-amplitude afterhyperpolarization than L2/3 neurons (Figure 1G; at 400 pA: $L2/3_{AHP}$ = 0.56 ± 0.12 mV, n = 10 cells versus $L5_{AHP}$ = 2.42 ± 0.17 mV, n = 22 cells; p < 0.001). Overall, our data show distinct intrinsic membrane properties of forepaw S1 L5 and L2/3 neurons.

Layer-Specific V_m Dynamics during Forepaw Behavior

We next compared the V_m properties and dynamics of L2/3 and L5 neurons during forepaw behavior. Spontaneous digit movements were monitored by the sensing arm and used to define periods of quiet wakefulness (Q) and digit movement (M) (see Experimental Procedures). Q was characterized by large-amplitude, low-frequency V_m fluctuations observed in all recordings from neurons in both layers (Figure 2A). Slow fluctuations had a similar mean duration across layers (L2/3 329.06 ± 27.55 ms, n = 13 cells versus L5 266.94 ± 11.15 ms, n = 23 cells) but lower frequency in L2/3 (L2/3 2.03 ± 0.08 Hz, n = 13 cells versus L5 2.29 ± 0.04 Hz, n = 23 cell; p = 0.005) (Figure S1). In both layers, M was accompanied by a reduction in the amplitude of low-frequency fluctuations, with fast Fourier transform analysis highlighting a reduction in the power in the 1 to 5 Hz range (Figures 2B and 2C), and a reduction in the SD of the V_m (Figure 2D). Mean AP firing rates were higher in L5 than L2/3 neurons during Q (Figure 2E; $L2/3_{FR}$, Q = 0.32 ± 0.10 Hz, n = 12 cells versus $L5_{FR}$, Q = 2.86 ± 0.60 Hz, n = 19 cells; p < 0.001). Moreover, a significant increase in mean firing rates during M was observed in L5 neurons ($L5_{FR}$ Q = 2.86 ± 0.60 Hz versus M = 6.14 ± 1.16 Hz, n = 19 cells, p = 0.005), but not L2/3 ($L2/3_{FR}$ Q = 0.32 ± 0.10 Hz versus M = 0.45 ± 0.18 Hz, n = 12 cells; p = 0.851). Inter-spike intervals (ISIs) showed a skewed distribution in both layers, with ~22% of L2/3 APs and ~30% of L5 APs having an ISI of <25 ms (Figure S2). We next analyzed AP bursting and observed similar burst durations across layers but overall more busts in L5 neurons. No differences were observed between Q and M periods (burst frequency $L2/3_{BF}$, Q = 0.02 ± 0.004 Hz, M = 0.03 ± 0.01 Hz, n = 13 cells versus $L5_{BF}$, Q = 0.14 ± 0.05 Hz, M = 0.25 ± 0.12 Hz, n = 23 cells, L2/3 versus L5 Q, p = 0.019; Figure S2).

To investigate what drove the laminar differences in mean AP rates, we next examined the AP threshold. AP threshold in L2/3 and L5 neurons varies dependent on the speed of pre-spike depolarization in V_m, with faster depolarizing ramps evoking APs at lower threshold (Figure S3). There was, however, no overall difference in AP threshold between L2/3 and L5 neurons in Q or M periods (Figure 2F). Measurement of the mean V_m showed a depolarization during M in both L2/3 (Figure 2G; $L2/3_{Mean}$ Q = −56.92 ± 1.21 mV versus M = −51.45 ± 1.73 mV, n = 12 cells; p < 0.001) and L5 neurons ($L5_{Mean}$ Q = −50.70 ± 0.65 mV versus M = −45.89 ± 0.80 mV, n = 19 cells; p < 0.001), with L5 neurons significantly more depolarized in both behavioral states (Q $L2/3_{Mean}$ versus $L5_{Mean}$ p < 0.001; M = $L2/3_{Mean}$ versus $L5_{Mean}$ p = 0.006). Notably, plotting the mean spontaneous AP rates as a function of the difference between AP threshold and the mean value of the top 10% of the V_m distribution (max V_m) revealed an exponential decay (Figure 2H). L5 neurons were distributed on the falling slope and L2/3 on the tail of the slope (Figure 2H), suggesting that the simplest explanation for higher firing rates in L5 neurons is their more depolarized V_m. Most likely, this works in combination with the higher input resistance of L5 neurons (Figure 1) to push excitatory postsynaptic potentials over AP threshold and trigger more APs in L5 than L2/3 neurons in behaving mice.

V_m Synchrony across Cortical Layers Is Regulated by Behavioral State

Synchrony of cortical activity across layers is thought to be an important feature of cortical coding. To examine translaminar subthreshold and spiking synchrony, we next inserted two pipettes through neighboring craniotomies to target recording sites in the same vertical axis and made nine simultaneous, dual whole-cell recordings from L2/3 and L5 neurons (Figure 3A). We went on to measure V_m synchrony at different timescales using cross-correlation, coherence analysis, and spike-triggered averaging.

Visual inspection of dual V_m recordings and cross-correlation analysis shows that large-amplitude slow fluctuations in resting mice are highly correlated across layers (Figures 3A–3E). As mice went from Q to M, however, the correlation of the V_m between L2/3 and L5 neurons was reduced in all pairs of cells (Figures 3D and 3E). Unexpectedly, the peak time of the cross-correlation showed a significant time lag, indicating that L5 subthreshold activity preceded that in L2/3 by 8.04 ± 1.40 ms in resting mice and by 4.35 ± 1.85 ms during M (Figure 3F). Coherence measurements suggested that the drop in correlation during M was due mostly to the reduction in low-frequency (1–5 Hz) coherence (Figures 3G and 3H). Thus, dual whole-cell recordings showed that subthreshold activity of cortical neurons in awake animals is under dynamic control, with cortical layers becoming more independent during active brain states.

To quantify AP synchrony from dual recordings, we made spike-triggered peri-stimulus time histograms (PSTHs) of spontaneous APs. The chance of observing an AP in a L5 neuron in a 10-ms window around a L2/3 AP is 6.1% during Q and 5.6% during M, and the chance of observing an AP in a L2/3 neuron around a L5 AP is 1.0% during Q and 0.4% during M. Thus, while the chance of observing an AP is dependent upon the firing rate, AP firing appears asynchronous at fast timescales across cortical L2/3 and L5 in awake mice. We next examined the synaptic input driving spontaneous APs. In both layers, APs were triggered by large-amplitude and cell-specific depolarizing synaptic input (Figures 3I–3K). At the time of the AP, a slow, small-amplitude depolarization was observed in the simultaneously recorded cell in resting mice, necessarily induced by the slow network fluctuations. A similar picture was present during movement: APs were triggered by large-amplitude, depolarizing inputs in the spiking cell that were absent in the simultaneously recorded neuron. These observations provide a synaptic basis for independent laminar spontaneous firing and suggest that

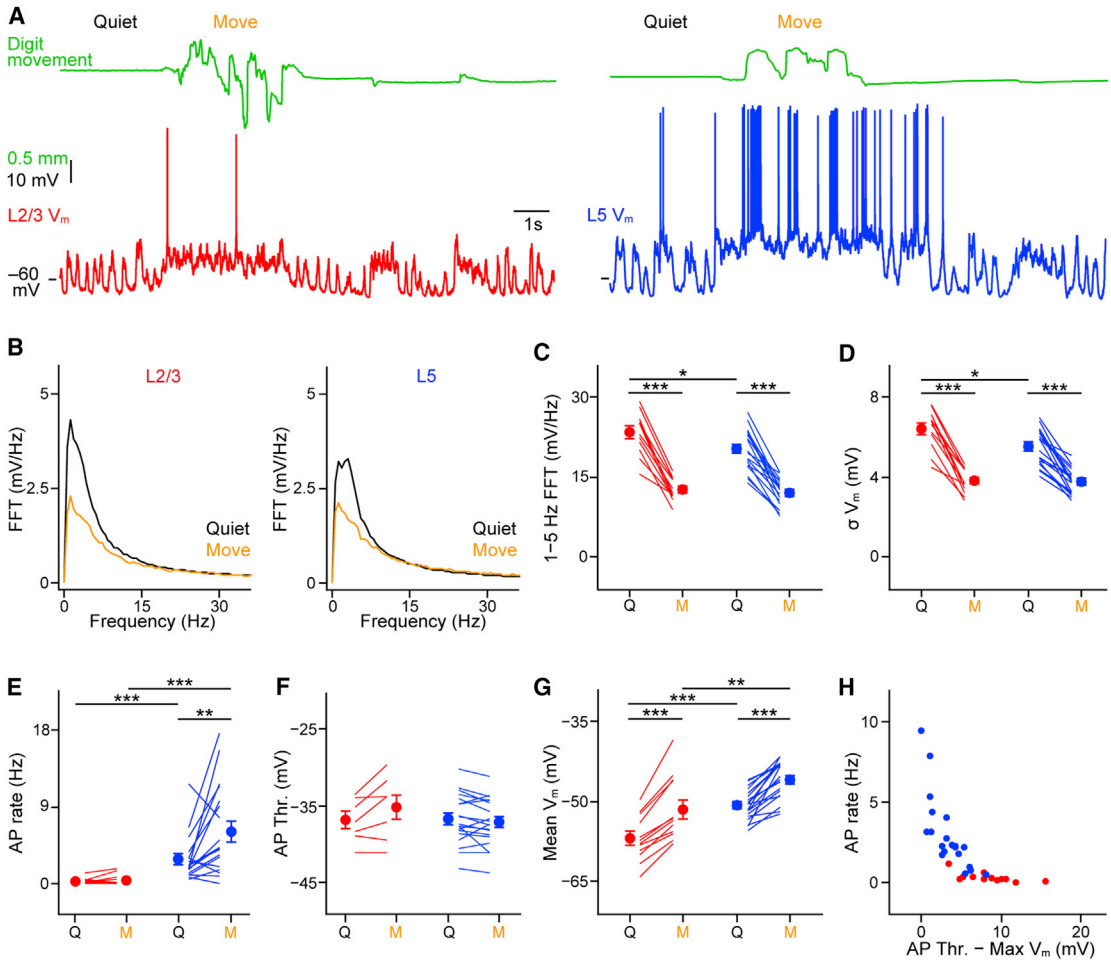

Figure 2. Laminar-Specific V_m Dynamics of L2/3 and L5 Neurons during Forepaw Behavior

(A) Example whole-cell recordings from a L2/3 neuron (red) and L5 neuron (blue) with the digit movement (green) measured by the stimulator/sensing arm in contact with the glabrous skin of forepaw digit 3.

(B) Population average fast Fourier transforms (FFTs) of the V_m of L2/3 and L5 neurons during quiet wakefulness (black) and digit movement (orange).

(C) Power of low-frequency activity (1–5 Hz) in the quiet (Q) and moving (M) state shows a significant reduction during digit movement in both L2/3 and L5 neurons. Filled circles with error bars show mean ± SEM, and lines represent individual neurons.

(D) SD of the V_m was significantly reduced during forepaw movement in both L2/3 and L5 neurons.

(E) L5 neurons showed an overall higher AP firing rate than L2/3 neurons in quiet and moving mice and a significant increase in AP firing rate during movement.

(F) AP threshold was not significantly different at rest and during movement in L2/3 and L5 neurons.

(G) Both L2/3 and L5 neurons depolarize during digit movement, but L2/3 neurons are more hyperpolarized than L5 neurons in both behavioral states.

(H) The mean firing rate (Q and M periods) of L2/3 and L5 neurons plotted as a function of the distance between AP threshold and the mean value of the maximum 10% of the V_m (Max V_m). Filled circles show the mean value for one cell.

For all panels, *$p < 0.05$, **$p < 0.01$, and ***$p < 0.001$. See also Figures S1–S3.

spontaneous AP firing in L2/3 and L5 excitatory neurons is driven by sparsely connected excitatory networks.

L5 Neurons Show an Earlier Onset of Slow Spontaneous Fluctuations

The time lag of the cross-correlation analysis and independent synaptic input during spiking suggested that there might be laminar differences in the fine temporal structure of spontaneous subthreshold fluctuations. We therefore first compared the onset timing of the slow depolarizing fluctuations in resting mice from dual L2/3 and L5 recordings (Figures 4A and 4B). We defined a slow depolarizing event (SDE) as depolarizing epochs in Q periods whose average V_m level between onset and offset was >60% of the V_m range between the most hyperpolarized and depolarized values for at least 100 ms. Plotting the duration and V_m of isolated SDEs across seven dual recordings as a heatmap (Figures 4B and S4) revealed a range of durations with a mean of ~300 ms (Figure S1B for single and dual recordings, L2/3 = 329.06 ± 27.55 ms, n = 13 cells, L5 = 266.94 ± 11.15 ms, n = 23 cells, $p = 0.086$). Normally a SDE in one neuron was accompanied by a SDE in the simultaneously recorded neuron, but a minority of small-amplitude, short-duration SDEs were observed in one layer only

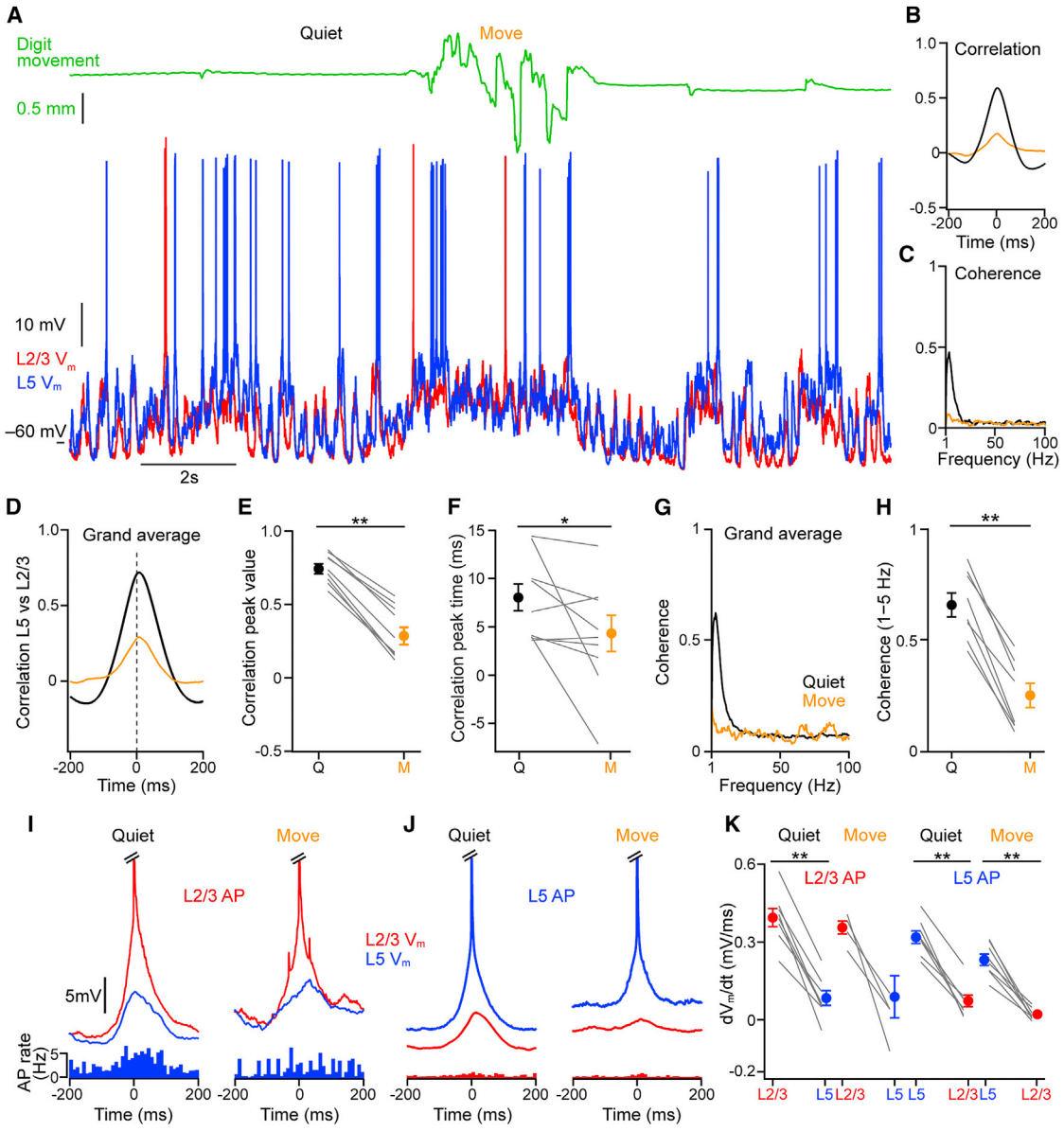

Figure 3. V_m Synchrony between L2/3 and L5 Neurons Is Dependent on Behavioral State

(A) Example dual whole-cell recording from a L2/3 (red) and a L5 (blue) cortical neuron during digit movement (green).

(B) Mean cross-correlation for the example recording shown in (A), taking L5 as the reference, shows a higher correlation during quiet (Q) than digit movement (M).

(C) Example mean coherence spectrum from the example recording shown in (A) from Q and M periods.

(D) Population mean cross-correlation (n = 9 pairs) during Q and M periods.

(E) Significant reduction in the peak cross-correlation value in M compared to Q periods. Filled circles with error bars show mean ± SEM, lines show data from individual pairs.

(F) The peak time of the cross-correlation shows a positive lag indicating that L5 neurons are active before L2/3 neurons in Q and M periods.

(G) Population mean average of coherence spectrum during Q and M periods (n = 8 pairs).

(H) A significant reduction in coherence from Q to M periods in frequency band 1–5 Hz.

(I) Population V_m average of L2/3 (red) and L5 neurons (blue) centered on APs in L2/3 neurons during quiet (left, n = 8 pairs) and moving (right, n = 4 pairs) periods. Bottom, corresponding population L5 spike-time PSTHs.

(J) Same as (I) but for L5 spike-triggered averages with L2/3 PSTH below (n = 8 pairs).

(K) Quantification of the V_m rise time in L2/3 and L5 neurons between −22 ms and −2 ms before a (left) L2/3 AP and (right) L5 AP in quiet and moving periods. Filled circles show population mean with error bars showing mean ± SEM. Gray lines show values from individual cells.

For all panels, *p < 0.05, **p < 0.01, and ***p < 0.001.

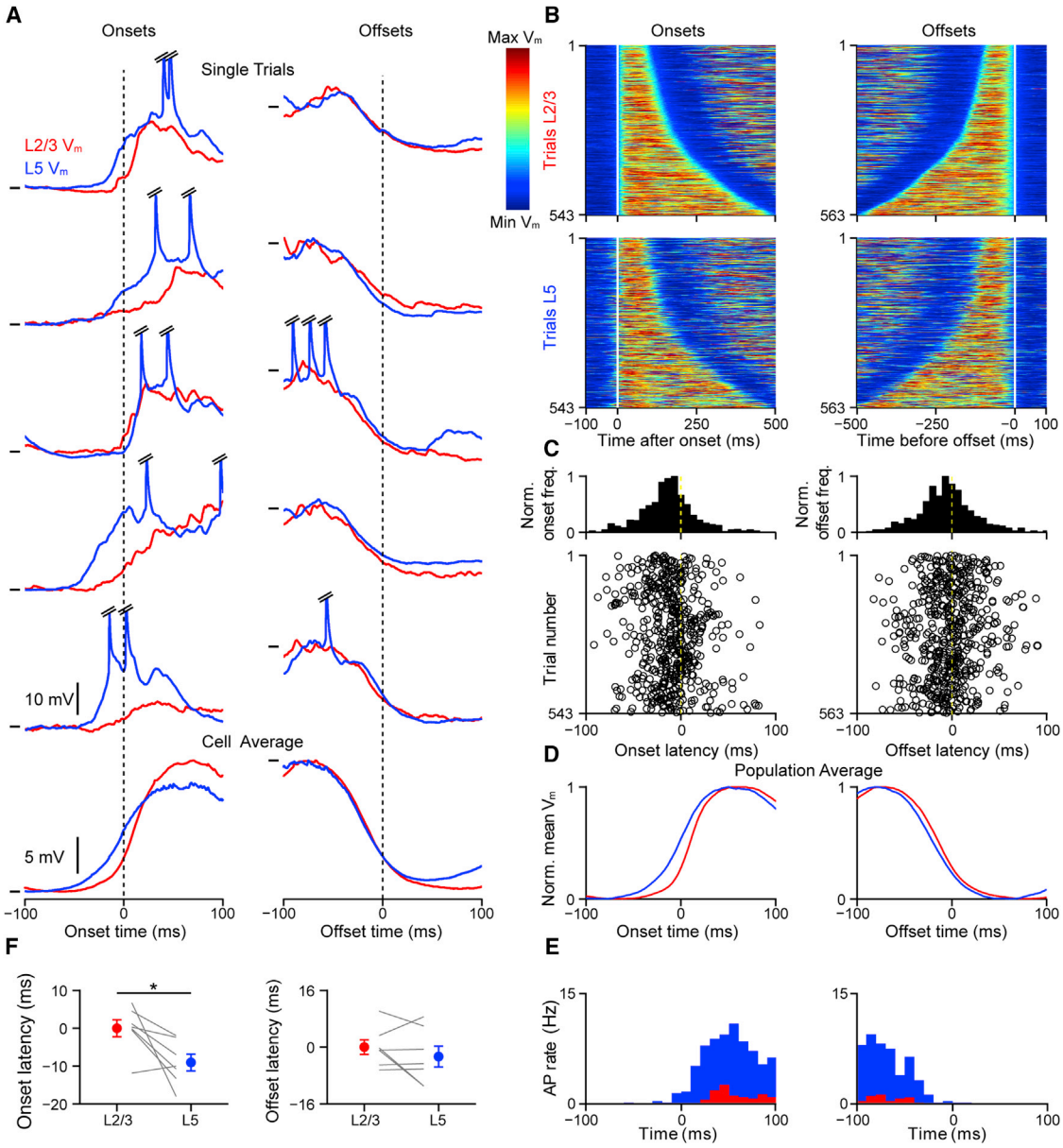

Figure 4. Slow Depolarizing Fluctuations during Quiet Wakefulness Have an Earlier Onset in L5 Neurons

(A) Example slow depolarizing events (SDEs) from a dual L2/3 (red) and L5 (blue) whole-cell recording in an awake, resting mouse. V_m traces are aligned to the onset (left) and offset (right) of the SDE in the L2/3 neuron, and bottom traces show V_m averages. Note that L5 leads at the onset, but not the offset, of the SDEs. Horizontal lines indicate V_m (mV) for L2/3 and L5 (trial 1 onset, −69.3/−63.1 mV and offset, −47.7/−44.7 mV; trial 2 onset, −59.3/−59.1 mV and offset, −40.0/−37.7 mV; trial 3 onset, −60.9/−57.0 mV and offset, −31.8/−31.7 mV; trial 4 onset, −59.7/−56.4 mV and offset, −42.0/−37.7 mV; and trial 5 onset, −58.3/−55.7 mV and offset, −40.0/−30.1 mV). Average onset, −60.0/−52.6 mV and offset, −41.9/−37.0 mV. APs have been truncated.

(B) Plots of selected SDEs from seven dual whole-cell recordings. SDEs were aligned at threshold crossing at the onset (left) and offset (right) of the SDE in the L2/3 neuron and arranged by duration. Top boxes show L2/3 data, and bottom boxes show L5 with colors corresponding to the normalized V_m from minimum (blue) to maximum (red) values.

(C) Population distribution (top) and trial-by-trial measurements (bottom) of the subthreshold onset (left) and offset (right) times in L5 neurons relative to the onset and offset times in L2/3, respectively (n = 7 dual recordings). Onset and offset times were estimated by the 5% level of a sigmoidal fit to the V_m at onset and offset (see Supplemental Experimental Procedures for details).

(D) Population average of the normalized V_m SDEs in L2/3 and L5 relative to the threshold-crossing at onset and offset of the L2/3 neuron.

(E) Population peri-SDE time histogram of AP times from the dataset used in (D).

(F) Population analysis of onset and offset times relative to the L2/3 SDE shows a significantly earlier onset in L5 but similar offset times. To calculate the onset/offset timing difference, we first measured the time of SDE onset/offset relative to the time of threshold crossing of the L2/3 SDE. Then, we subtracted the population mean L2/3 onset/offset time from all values. Filled circles with error bars show mean ± SEM, and lines show data from individual pairs.

For all panels, *p < 0.05, **p < 0.01, and ***p < 0.001. See also Figures S4 and S5.

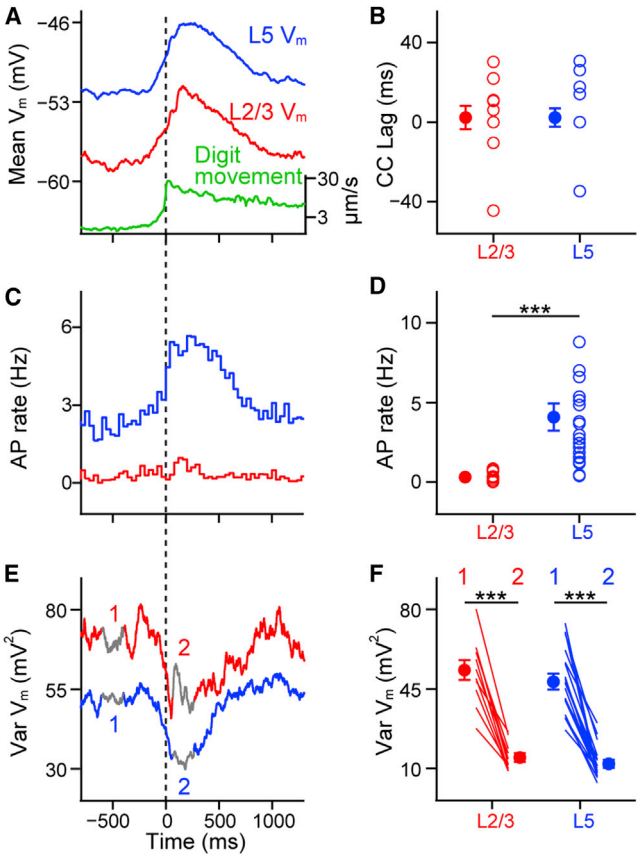

Figure 5. Movement Onset Synchronizes Synaptic Input across Layers and Results in an Increase in L5 AP Rate

(A) Population V_m average responses of L2/3 (red) and L5 (blue) neurons to onset of spontaneous digit movement (green shows the rectified first derivative of the digit movement ($digit_{FD}$); n = 11 L2/3 cells and n = 19 L5 cells, from single and dual recording experiments). Movement onsets (dashed vertical line) were detected via thresholding of $digit_{FD}$ (see Experimental Procedures).

(B) Peak cross-correlation between the $digit_{FD}$ and the V_m shows no significant time lag between layers, indicating synchronous depolarization. Filled circles with error bars show mean ± SEM, and open circles show individual cells.

(C) Mean population AP rates over time with respect to movement onset from L2/3 and L5 neurons.

(D) L5 neurons show a significantly higher AP firing rate after movement onset (between 0 and 1 s) than L2/3 neurons.

(E) Population average of the variance of the V_m over time with respect to movement; gray sections and numbers show time points for analysis in (F).

(F) L2/3 and L5 neurons show a significant reduction in the V_m variance following movement onset; the two measurement time windows (1 and 2) are indicated in (E).

For all panels, *p < 0.05, **p < 0.01, and ***p < 0.001.

(Figure S5), likely accounting for the slightly shorter durations of SDEs in L5. In those SDEs with a measureable V_m onset in both layers, plotting the trial-by-trial onset times (Figure 4C; Supplemental Experimental Procedures), the population averaged V_m (Figure 4D) and population spiking rates (Figure 4E) revealed that L5 SDEs started earlier than those in L2/3 (Figure 4F; L5 leading L2/3 = 9.07 ± 2.19 ms, n = 7 pairs, p = 0.031). In contrast, the hyperpolarizing offset time was not significantly different across layers when SDEs were triggered on L2/3 onset (Figures 4A and 4F). SDEs thus have an earlier onset in higher-firing L5 neurons, supporting the proposal that L5 neurons are important drivers of supragranular slow network activity (Beltramo et al., 2013; Sanchez-Vives and McCormick, 2000).

Movement Onset Triggers Synchronous Input across Layers

Is the laminar-specific synaptic input observed during AP firing (Figure 3) and spontaneous activity (Figure 4) a general feature of subthreshold processing in cortical neurons, or are there other sources of more synchronized synaptic input? Movement triggers an active, desynchronized cortical state, which can be driven by thalamic input (Poulet et al., 2012). To examine the fast dynamics of movement related synaptic input across layers, we next analyzed the V_m dynamics at M onset (detected by thresholding the first derivative of the digit movement signal; Supplemental Experimental Procedures). Averaging the V_m showed that M onset is accompanied by simultaneous depolarizing synaptic input to L2/3 and L5 neurons (Figures 5A and 5B). Close inspection of the log-scale digit movement trace indicated that the depolarization in both layers was tightly coupled to the tiny initial movements of the digits and did not appear before movement. To quantify the timing of the depolarization, we performed cross-correlation analysis between the averaged digit movement and the averaged V_m response at M onset. The peak of the cross-correlation showed no significant time lag (Figure 5B), suggesting an internal, non-sensory origin for synaptic input at movement onset.

Analysis of 2-s epochs of V_m activity showed an overall reduction in the SD of the V_m during extended M periods (Figure 2), but how fast this occurs was unclear. We therefore quantified the variance of the L2/3 and L5 subthreshold activity around all recorded M onsets, including short-duration movements (Figures 5E and 5F). In all cells across both layers, we observed a rapid and robust reduction in variance within the first 200 ms of movement onset. Thus, early movement-evoked input acts to reduce subthreshold variability simultaneously across cortical layers. The reduction in variance, however, does not result in synchronous AP firing. Instead, L5 neurons showed higher firing rates after movement onset than L2/3 neurons (Figures 5C and 5D). Thus, unlike the laminar-specific V_m dynamics during SDEs and spontaneous APs, movement onset triggers simultaneous V_m depolarization across layers, which results in an increase in firing only in L5 neurons.

Tactile Stimulation Evokes Correlated Synaptic Input across Layers

Another major source of synaptic input to S1 is sensory-evoked thalamic input. Thalamo-cortical axons are unequally distributed across the cortical layers, with some L5 neurons receiving direct thalamic input (Bureau et al., 2006; Constantinople and Bruno, 2013). We therefore next examined whether there is laminar specificity in sensory processing across layers in behaving animals. We delivered brief (2 ms), light (10 mN) tactile stimuli via the stimulating/sensing arm to digit 3 during single and dual whole-cell recordings. The sensing arm was in constant contact with the glabrous skin of digit 3. Tactile stimulation evoked a subthreshold response in all cells. While the first spike latency was similar for both behavioral conditions and layers

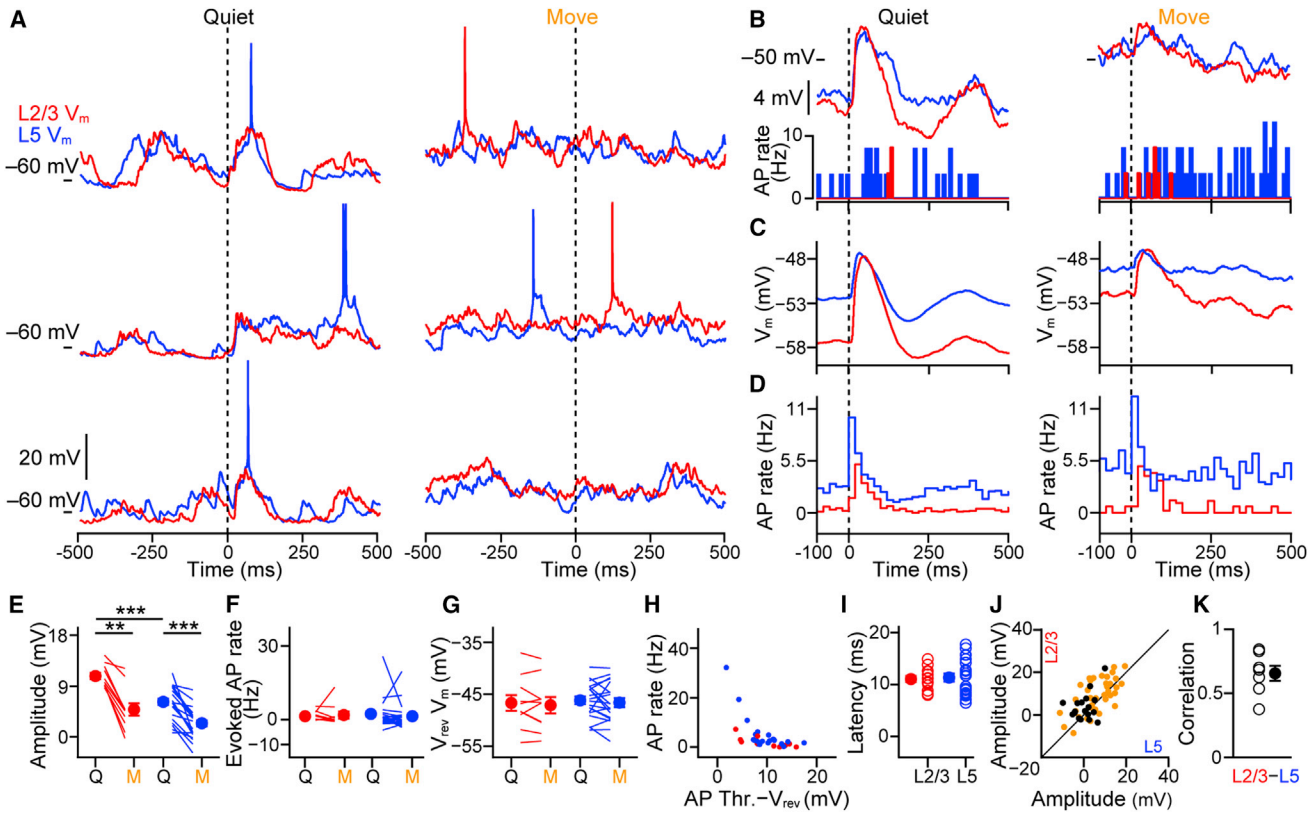

Figure 6. Tactile-Evoked Subthreshold Responses Are Highly Correlated across Cortical Layers and Modulated by Behavioral State

(A) Single-trial tactile-evoked responses from a dual L2/3 (red) and L5 (blue) whole-cell recording during quiet wakefulness (left) and movement (right).

(B) Top: mean V_m tactile-evoked response of example neurons in (A) during quiet wakefulness and movement shows reduction in amplitude during moving periods. Bottom: corresponding PSTH of AP firing.

(C) Population averaged subthreshold tactile-evoked response during quiet wakefulness and movement.

(D) Population PSTH from L2/3 and L5 to tactile stimulation during quiet wakefulness and movement.

(E) L2/3 and L5 neurons show a decrease in tactile-evoked subthreshold response amplitude as mice go from quiet (Q) to movement (M). Filled circles with error bars show mean ± SEM. Lines show individual cells.

(F) Population analysis of background-subtracted AP firing rates to tactile stimulation of the forepaw shows no difference between Q (left) and M (right) periods in both layers. AP rate measured as the difference between the 100 ms before and 100 ms after stimulus onset.

(G) The subthreshold tactile-evoked reversal potential shows no significant difference between layers or behavioral states.

(H) Absolute AP rate in the 100 ms after stimulus onset plotted as a function of the difference in V_m between AP threshold and the tactile stimulus-evoked response reversal potential. Filled circles show mean value of individual cells.

(I) Subthreshold tactile-evoked response latencies of L2/3 and L5 neurons are not significantly different.

(J) Amplitude of L2/3 subthreshold tactile-evoked responses plotted against the amplitude of L5 subthreshold responses from the example pair in (A) shows highly correlated response amplitudes during Q (black) and M (orange) periods.

(K) Population data of cross-correlation of mean subthreshold tactile-evoked responses (combining Q and M responses) between L2/3 and L5 neurons. Filled circles with error bars show mean ± SEM, and open circles show individual cells.

For all panels, *p < 0.05, **p < 0.01, and ***p < 0.001. See also Figures S6 and S7.

(Figure S6B), the amplitude of the V_m response was strongly dependent on the behavioral state (Figures 6A–6D). In Q periods, stimuli evoked a large-amplitude depolarizing response in both layers, whereas the amplitude of the response was reduced during M (Figures 6C and 6E; $L2/3_{Amp}$ Q = 10.80 ± 0.65 mV, M = 4.84 ± 1.24 mV, n = 10 cells, p = 0.037; $L5_{Amp}$ Q = 6.19 ± 0.69 mV, M = 2.41 ± 0.60 mV, n = 20 cells, p = 0.001; Q $L2/3_{Amp}$ versus $L5_{Amp}$ p < 0.001, and M $L2/3_{Amp}$ versus $L5_{Amp}$ p = 0.005). Despite the difference in subthreshold response amplitude, tactile stimulation evoked few extra APs over the background rate in both layers in both behavioral conditions (Figures 6D, 6F, and S6A; $L2/3_{AP}$ Q = 1.59 ± 0.62 Hz, M = 1.95 ± 1.36 Hz, n = 10 cells, p = 0.375; $L5_{AP}$ Q = 2.44 ± 1.40 Hz, M = 1.55 ± 1.16 Hz, n = 20 cells, p = 0.370; Q $L2/3_{AP}$ versus $L5_{AP}$ p = 0.613, M $L2/3_{AP}$ versus $L5_{AP}$ p = 0.523)

To examine why L5 neurons do not fire more APs in response to tactile stimulation despite having a more depolarized V_m, we measured the tactile responses as a function of the V_m just prior to stimulus onset. As neurons became more depolarized, the sensory response reduced in amplitude until eventually showing a hyperpolarizing response (Figure S7). The V_m level for the tactile-evoked reversal potential was similar during Q and M

periods and hyperpolarized relative to glutamate reversal potential (Figure 7G, $L2/3_{Rev}$ Q = −46.67 ± 1.60 mV, M = −47.09 ± 1.59 mV, n = 10 cells, p = 0.492; $L5_{Rev}$ Q = −46.17 ± 0.75 mV, M = −46.61 ± 0.86 mV, n = 20 cells, p = 0.412; Q $L2/3_{Rev}$ versus $L5_{Rev}$ p = 0.644, M $L2/3_{Rev}$ versus $L5_{Rev}$ p = 0.775). Notably, a minority of cells with higher mean firing rates showed a smaller difference between AP threshold and the sensory reversal potential (Figure 6H). These data provide an explanation for why the evoked rates are similar across layers and suggest that sensory-evoked GABA-ergic inhibition plays a critical role in defining the sensory reversal potential in both layers (Crochet et al., 2011; Moore and Nelson, 1998).

We next examined correlations between the timing and amplitude of sensory-evoked synaptic responses across layers during dual recordings. While the onset latencies of the synaptic and spiking responses to tactile stimulation in L5 neurons were more broadly distributed than in L2/3, there was no significant difference across layers (Figure 6I, $L2/3_{PSPLat}$ = 11.07 ± 0.58 ms, n = 13 versus $L5_{PSPLat}$ = 11.34 ± 0.76 ms, n = 21, p = 0.972; Figure S6B, $L2/3_{1stAPLat,}$ Q = 33.78 ± 4.73 ms, n = 8 cells, M = 44.67 ± 8.30 ms, n = 3 cells; $L5_{1stAPLat,}$ Q = 39.52 ± 4.72 ms, n = 19 cells, M = 31.10 ± 5.90 ms, n = 9 cells). Moreover, trial-by-trial analysis of the tactile-evoked postsynaptic potential (PSP) showed that subthreshold response amplitudes were highly correlated between L2/3 and L5 neurons (Figures 6J and 6K). Together, these data indicate that, in contrast to SDEs and spontaneous APs, tactile stimulation, like movement onset, triggers synchronized subthreshold input across layers.

L5 Neurons Signal Tactile-Triggered Movements

Following 75.2% of stimuli delivered in Q periods, the mouse's forepaw remained stationary (quiet-quiet [QQ] trials). However, 24.8% of stimuli in Q periods evoked short-latency (<100 ms) forepaw digit movements (Figure 7), termed quiet-move (QM) trials. We next compared sub- and supra-threshold responses in QQ with QM trials (Figures 7A–7C). Tactile stimulation evoked a short-latency, large-amplitude subthreshold response in QQ and QM trials in both layers (Figures 7A and 7B). Notably, the amplitude of the subthreshold response was larger in QM than QQ trials in both layers (Figure 7D; L2/3 QQ = 10.80 ± 0.65 mV versus QM = 11.83 ± 0.79 mV, n = 10 cells, p = 0.037; L5 QQ = 6.19 ± 0.69 mV versus QM = 8.16 ± 0.78 mV, n = 20 cells, p = 0.002; and QQ L2/3 versus L5 p < 0.001, QM L2/3 versus L5 p = 0.005). Moreover, we observed that the V_m prior to stimulus onset was significantly more hyperpolarized in QM trials than QQ trials in L5, but not in L2/3 neurons (Figures 7E; L2/3 QQ = −57.37 ± 1.36 mV, QM = −58.19 ± 1.58 mV, n = 10 cells, p = 0.232; L5 QQ = –52.53 ± 0.69 mV, QM = −54.24 ± 0.61 mV, n = 20 cells, p = 0.009; and QQ L2/3 versus L5 p = 0.006, QM L2/3 versus L5 p = 0.033). In QQ trials, the peak response was then followed by a brief hyperpolarization and subsequent depolarization peaking at ~350 ms (Figure 7B). This secondary depolarization was significantly larger in both layers during QM than QQ trials (Figure 7F) and evoked APs in L5, but not L2/3, neurons (Figures 7C and 7G; L2/3 QQ = −0.18 ± 0.13 Hz, QM = −0.12 ± 0.34 Hz, n = 10 cells, p = 0.910; L5 QQ = −0.01 ± 0.24 Hz, QM = 2.66 ± 0.81 Hz, n = 20 cells, p = 0.003; QQ L2/3 versus L5 p = 0.613, QM L2/3 versus L5 p = 0.011). Thus, movements evoked by a tactile input are linked to a more hyperpolarized pre-stimulus V_m, a larger subthreshold early response, and a higher late increase in mean firing rate of L5 neurons.

DISCUSSION

The coordinated activity of six layers of primary sensory cortical neurons underlies sensory perception. Using whole-cell recordings in awake mice, we investigated synaptic mechanisms of translaminar synchronous activity. We show that laminar-specific differences in membrane properties drive distinct firing rates, that translaminar synchrony is dependent both on the behavioral state and the source of synaptic input (spontaneous, sensory, and movement evoked), and that L5 neurons signal spontaneous and tactile-triggered movement.

V_m Determinants of Spontaneous AP Firing Rates

Prior work has observed low firing rates of L2/3 excitatory neurons during synchronized states in resting and anesthetized animals (Barth and Poulet, 2012; Jouhanneau et al., 2014) and no change (Crochet and Petersen, 2006; Polack et al., 2013; Poulet and Petersen, 2008; Zhou et al., 2014) or a reduction (Bennett et al., 2013; Sakata and Harris, 2012) of firing rates during activated cortical states. We observed that L5 neurons have a higher mean spontaneous rate of APs (2.86 ± 0.60 Hz) than L2/3 neurons (0.32 ± 0.09 Hz) in resting mice, supporting previous reports in anesthetized and awake animals (Brecht et al., 2003; Constantinople and Bruno, 2011; de Kock et al., 2007; de Kock and Sakmann, 2009; Manns et al., 2004; O'Connor et al., 2010; Sakata and Harris, 2009), and, in contrast to L2/3, a significant increase in mean firing rates during movement (Figure 2). Previous studies of deeper layers have observed both increases and decreases in firing rates of somatosensory (Curtis and Kleinfeld, 2009; de Kock and Sakmann, 2009) and motor (Carvell et al., 1996; Schiemann et al., 2015; Zagha et al., 2015) cortical neurons during movement.

What synaptic and cellular mechanisms could explain the higher firing rates in L5 neurons? Our whole-cell recordings indicate that higher L5 rates were not the result of an intrinsic difference in AP threshold. Moreover, AP triggered averaging showed that the depolarizing synaptic inputs driving APs had similar amplitudes and dynamics in L2/3 and L5 neurons (Figure 3). Instead, higher mean firing rates in L5 neurons appeared to result from a larger input resistance and a more depolarized V_m, as observed in subsets of L5 pyramidal neurons in vitro (Lefort et al., 2009; Mason and Larkman, 1990), which likely combine to push excitatory input over AP threshold more often than in L2/3 neurons. Because most excitatory connections to pyramidal neurons are small in amplitude (Jouhanneau et al., 2015; Lefort et al., 2009) and the rise time of the depolarization prior to an AP is negatively correlated with AP threshold (Figure S3) (Azouz and Gray, 2000; Poulet and Petersen, 2008), it is likely that coincident synaptic input is required to drive spontaneous AP firing in both layers.

Sensory-Evoked Firing Rates Are Determined by a Hyperpolarized Reversal Potential

In resting mice, the absolute tactile-evoked firing rate was higher in L5 (5.03 ± 1.74 Hz) than L2/3 (1.96 ± 0.75 Hz) neurons, but this

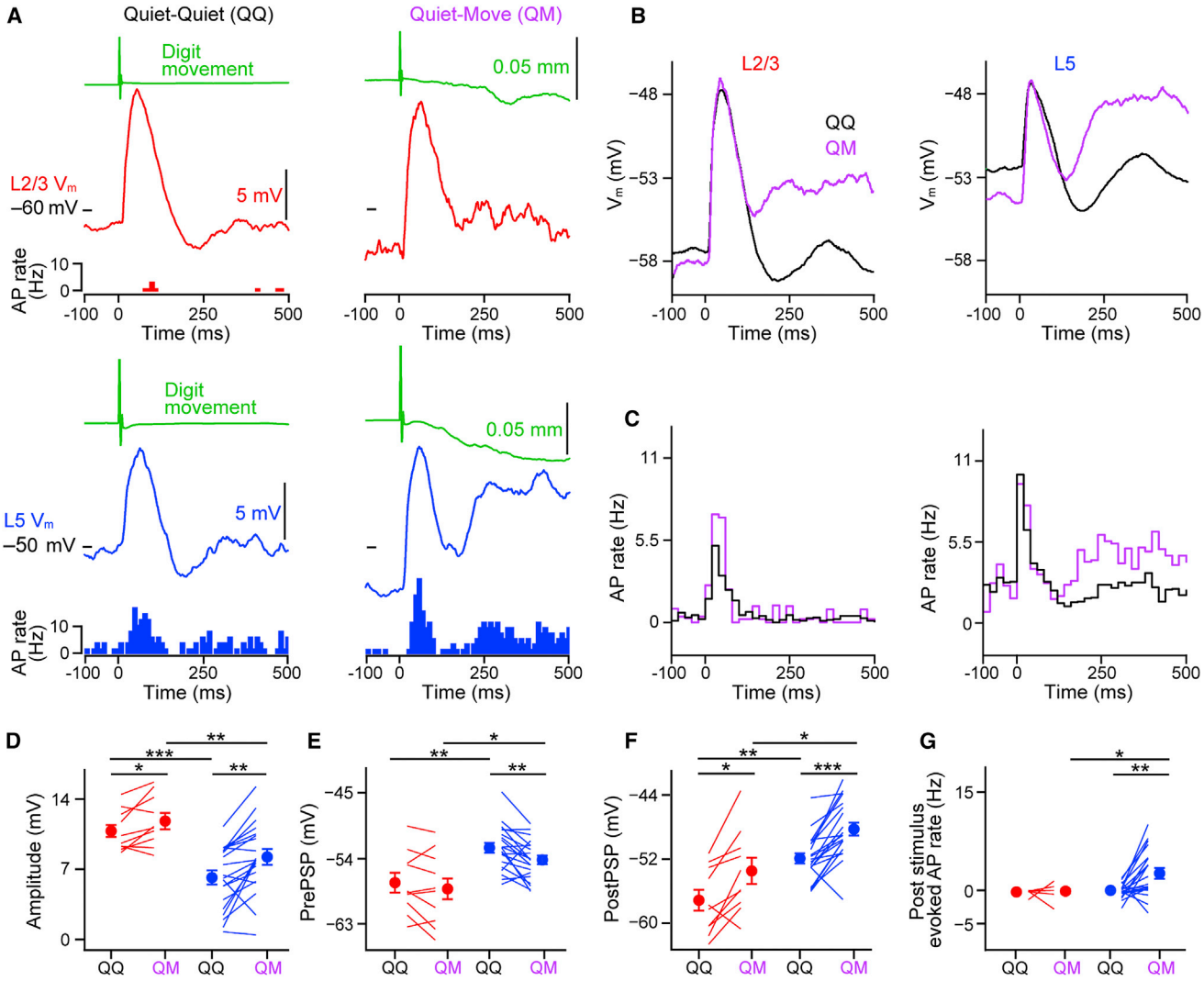

Figure 7. Tactile-Evoked Forepaw Movements Are Signaled by L5 Neurons

(A) Mean V_m tactile-evoked responses with corresponding digit movement (green) and PSTHs from an L2/3 (red, top) and an L5 (blue, bottom) neuron in resting, quiet mice that showed no behavioral response (left, quiet-quiet [QQ]) or a short-latency digit movement following the stimulus (right, quiet-movement [QM]).

(B) Grand average tactile-evoked responses from all L2/3 and L5 neurons during QQ and QM trials.

(C) Population PSTHs of firing rates in L2/3 and L5 neurons following tactile stimulation in QQ and QM trials. Note that only L5 neurons show an evoked spiking response in the later phase (300–400 ms after stimulus onset).

(D) The amplitude of the V_m response to tactile stimulation is significantly larger for QM trials than in QQ trials in both L2/3 and L5 neurons. Filled circles with error bars show mean ± SEM. Lines show individual cells.

(E) The mean V_m in the 100 ms before stimulus onset is more hyperpolarized in QM trials than QQ trials in L5, but not in L2/3 neurons.

(F) The mean V_m in the late phase (300–400 ms following tactile stimulation) is significantly more depolarized after a QM trial than a QQ trial in both layers.

(G) Significant increase (background subtracted) in AP firing rates in QM trials as compared to QQ trials in the late phase (300–400 ms following tactile stimulation) in L5 neurons, but not in L2/3 neurons.

For all panels, *$p < 0.05$, **$p < 0.01$, and ***$p < 0.001$.

was superimposed on different background firing rates. In fact, a brief tactile stimulus added similarly few additional APs to the background rate in both layers (evoked rate: L2/3 1.59 ± 0.62 Hz and L5 2.44 ± 1.40 Hz). Our observation of low evoked rates across layers is similar to prior studies of S1 in anesthetized animals (Barth and Poulet, 2012; Brecht et al., 2003; de Kock et al., 2007; Manns et al., 2004). Higher evoked rates have been observed in "thick tufted" L5 pyramidal neurons (de Kock et al., 2007; Sakata and Harris, 2009). We did not differentiate between subtypes of cortical excitatory L5 neurons, but we did observe a minority (3/20) of L5 neurons with sensory-evoked rates >10 Hz (Figure 6F). Future work targeting whole-cell recordings to within-layer excitatory neuron subtypes in sensory cortex will be of great importance.

Cortical sensory responses are modulated by behavioral state in different sensory systems (Bennett et al., 2013; Crochet and Petersen, 2006; Niell and Stryker, 2010; Otazu et al., 2009; Schneider et al., 2014; Zhou et al., 2014). We report a reduction in subthreshold response amplitude in L2/3 neurons to brief tactile stimuli during movement. We go on to show that L5 neurons also have a reduced subthreshold response during movement (Figure 6). Despite this, the numbers of evoked APs remained the same in both layers during quiet and moving periods. In both layers, subthreshold responses were reduced in amplitude as the baseline V_m values became more depolarized and exhibited a reversal potential more hyperpolarized than AP threshold. Interestingly, in the cells with higher sensory-evoked firing rates, the sensory reversal potential was closer to threshold. Together, this suggests that strong, local GABAergic inhibition plays a significant role in clamping the subthreshold sensory response below AP threshold and regulating AP firing during behavior in both L2/3 (Crochet et al., 2011) and L5 neurons.

Correlated Neural Activity across Cortical Layers

Synchronous activity in cortical networks is thought to be fundamental to sensory processing and perception. Prior work has shown that spontaneous V_m activity in L2/3 neurons during resting states is more correlated than in activated states in behaving or attentive animals (Okun et al., 2010; Poulet and Petersen, 2008). We observed a similar pattern across L2/3 and L5. Neurons showed large-amplitude, highly correlated fluctuations of the V_m during resting periods and an active state with low SD, as well as a reduction in slow fluctuation amplitude and translaminar V_m synchrony (Figures 2 and 3). However, close inspection of the fine timing of subthreshold inputs evoked at different time points revealed differences in the timing of synaptic input across layers. Spontaneous APs were driven by cell-specific, depolarizing inputs (Figure 3). In contrast, movement- (Figure 5) and sensory-driven (Figure 6) synaptic input had a similar timing across layers. Interestingly, slow subthreshold fluctuations in resting mice had an earlier onset in L5, reminiscent of the earlier timing of "UPstate" onsets in deeper layers observed in anesthetized and sleeping animals (Chauvette et al., 2010; Sakata and Harris, 2009), cortical slices (Sanchez-Vives and McCormick, 2000), and extracellular recordings in awake rats (Sakata and Harris, 2009). Thus, the type of input (spontaneous, sensory, or movement evoked) determines the timing of synaptic input across layers.

What mechanisms could explain synaptic timing differences? One possibility is that they result from differences in the wiring supporting spontaneous, sensory, and motor events. In support of this suggestion, a recent anatomical study showed laminar differences in local and long-range cortico-cortical inputs to S1 excitatory neurons (DeNardo et al., 2015). Long-range inputs show laminar matching. L2/3 neurons receive proportionally more input from distant L2/3 neurons than L5 neurons, which receive a greater proportion from distant L5 neurons. Moreover, locally, L2/3 neurons receive a greater proportion of inhibitory inputs than L5 neurons. Upstates in anesthetized animals (Han et al., 2008; Luczak et al., 2007) and slow fluctuations in awake resting animals (Ferezou et al., 2007) are thought to propagate as waves of activity across cortex supported by long-range cortico-cortical connections. Thus, a later onset in L2/3 neurons could result from a combination of lower firing rates, increased inhibitory input, and laminar-specific cortico-cortical wiring. In contrast, because sensory thalamic neurons are driven both by sensory stimulation and movement (Poulet et al., 2012), we suggest that punctate thalamic input drives the synchronized synaptic input following tactile stimuli or movement onset.

L5 Neurons Report Spontaneous and Tactile-Evoked Movement

Subthreshold sensory responses are correlated not only with the behavioral and cortical state but also with the behavioral outcome. Both L2/3 and L5 neurons showed a larger-amplitude subthreshold sensory response in trials that lead to short-latency forepaw movements (QM trials) compared to trials with no movement before or after the stimulus (QQ trials). In L5 neurons, a difference was also observed in the pre-stimulus V_m, with QM trials having a more hyperpolarized value than QQ trials. This suggests that the link between subthreshold response amplitude and behavioral output is due to the prestimulus cortical state rather than delivery of different amplitude stimuli. Our findings resemble recent V_m recordings in auditory cortex during an auditory discrimination go/no-go task, where neurons from L4 and L5 showed more hyperpolarized V_m value in hit trials than in false-positive trials in mice performing an auditory perception task (McGinley et al., 2015). Future experiments could address whether this is the result of a higher signal to noise ratio in a phase of low network activity resulting in an enhanced probability of signal transmission to downstream motor centers.

During evoked movement trials, neurons in both layers showed a prominent late depolarization (Figure 7), with L5 neurons also showing an increase in late spiking. Because forepaw movements necessarily occurred soon after tactile stimulation in QM trials, it was difficult to assess whether the late activity is causally related to the perception of the stimulus (Sachidhanandam et al., 2013), an intrinsic part of the transformation of sensory input to motor output and/or the start of the active cortical state associated with attention or arousal. Examining mice trained to delay sensory-triggered movements will help link late activity to perception and movement.

Functional Consequences

We observed higher background firing rates in L5 neurons but no difference in the numbers of additional, sensory-evoked spikes across layers, suggesting that L2/3 and L5 have distinct sensory coding strategies (Sakata and Harris, 2009). The fine timing differences of synaptic input may be important in the processing of dynamic sensory stimuli and for changes of synaptic strength under spike-time-dependent plasticity rules. Fast, laminar-specific manipulations of synchronized activity in trained mice are now required to define the causal role of translaminar synchrony in perception.

EXPERIMENTAL PROCEDURES

All experiments were approved by the Berlin animal ethics committee and carried out in accordance with European animal welfare law. Head-restrained 6- to 9-week-old C57bl6J mice were paw-tethered, and digit movements were

monitored by a force-feedback sensing and stimulating arm. The sensing arm ending was a 4.7-mm-diameter flat disk with one edge pressed up against the glabrous skin of digit 3. Then, 2-ms, 10-mN tactile stimuli were delivered at pseudo-randomized intervals. Blind whole-cell patch-clamp recordings were made from primary somatosensory forepaw cortex located by intrinsic optical imaging. Neurons were processed for biocytin staining using standard histological techniques. Data were analyzed with custom-written scripts in MATLAB and IgorPro. All data were statistically analyzed using non-parametric tests, paired data with a Wilcoxon signed rank test and unpaired data with a Wilcoxon rank sum test. Data are presented as the mean ± SEM unless otherwise stated. See Supplemental Experimental Procedures for further details.

SUPPLEMENTAL INFORMATION

Supplemental Information includes Supplemental Experimental Procedures and seven figures and can be found with this article online at http://dx.doi.org/10.1016/j.celrep.2016.05.026.

AUTHOR CONTRIBUTIONS

W.-J.Z. and J.F.A.P. designed the project. W.-J.Z. performed all experiments. J.K. and W.-J.Z. analyzed the data. J.F.A.P. wrote the manuscript, with comments from all coauthors.

ACKNOWLEDGMENTS

We thank Janett König for technical help, Sven Blankenburg for help with coherence analysis, and Evgeny Bobrov, Jean-Sebastién Jouhanneau, and Birgit Voigt for comments on an earlier version of the manuscript. This work was funded by a European Research Council starting grant (ERC-2010-StG-260590, to J.F.A.P.), the Deutsche Forschungsgemeinschaft (DFG; Exc 257 NeuroCure, DFG-FOR-1341-BaCoFun and DFG-FOR-2143-Interneuron, to J.F.A.P.), the Fritz Thyssen Foundation, the European Union (3x3Dimaging 323945), and the Helmholtz Association. J.K. is funded by the Humboldt-Universität zu Berlin in the framework of the Excellence Initiative of the BMBF and DFG.

Received: December 16, 2015
Revised: March 24, 2016
Accepted: May 4, 2016
Published: June 2, 2016

REFERENCES

Azouz, R., and Gray, C.M. (2000). Dynamic spike threshold reveals a mechanism for synaptic coincidence detection in cortical neurons in vivo. Proc. Natl. Acad. Sci. USA *97*, 8110–8115.

Barth, A.L., and Poulet, J.F.A. (2012). Experimental evidence for sparse firing in the neocortex. Trends Neurosci. *35*, 345–355.

Beltramo, R., D'Urso, G., Dal Maschio, M., Farisello, P., Bovetti, S., Clovis, Y., Lassi, G., Tucci, V., De Pietri Tonelli, D., and Fellin, T. (2013). Layer-specific excitatory circuits differentially control recurrent network dynamics in the neocortex. Nat. Neurosci. *16*, 227–234.

Bennett, C., Arroyo, S., and Hestrin, S. (2013). Subthreshold mechanisms underlying state-dependent modulation of visual responses. Neuron *80*, 350–357.

Brecht, M., Roth, A., and Sakmann, B. (2003). Dynamic receptive fields of reconstructed pyramidal cells in layers 3 and 2 of rat somatosensory barrel cortex. J. Physiol. *553*, 243–265.

Bureau, I., von Saint Paul, F., and Svoboda, K. (2006). Interdigitated paralemniscal and lemniscal pathways in the mouse barrel cortex. PLoS Biol. *4*, e382.

Carvell, G.E., Miller, S.A., and Simons, D.J. (1996). The relationship of vibrissal motor cortex unit activity to whisking in the awake rat. Somatosens. Mot. Res. *13*, 115–127.

Castro-Alamancos, M.A. (2004). Absence of rapid sensory adaptation in neocortex during information processing states. Neuron *41*, 455–464.

Chauvette, S., Volgushev, M., and Timofeev, I. (2010). Origin of active states in local neocortical networks during slow sleep oscillation. Cereb. Cortex *20*, 2660–2674.

Constantinople, C.M., and Bruno, R.M. (2011). Effects and mechanisms of wakefulness on local cortical networks. Neuron *69*, 1061–1068.

Constantinople, C.M., and Bruno, R.M. (2013). Deep cortical layers are activated directly by thalamus. Science *340*, 1591–1594.

Crochet, S., and Petersen, C.C.H. (2006). Correlating whisker behavior with membrane potential in barrel cortex of awake mice. Nat. Neurosci. *9*, 608–610.

Crochet, S., Poulet, J.F.A., Kremer, Y., and Petersen, C.C.H. (2011). Synaptic mechanisms underlying sparse coding of active touch. Neuron *69*, 1160–1175.

Curtis, J.C., and Kleinfeld, D. (2009). Phase-to-rate transformations encode touch in cortical neurons of a scanning sensorimotor system. Nat. Neurosci. *12*, 492–501.

de Kock, C.P.J., and Sakmann, B. (2009). Spiking in primary somatosensory cortex during natural whisking in awake head-restrained rats is cell-type specific. Proc. Natl. Acad. Sci. USA *106*, 16446–16450.

de Kock, C.P.J., Bruno, R.M., Spors, H., and Sakmann, B. (2007). Layer- and cell-type-specific suprathreshold stimulus representation in rat primary somatosensory cortex. J. Physiol. *581*, 139–154.

DeNardo, L.A., Berns, D.S., DeLoach, K., and Luo, L. (2015). Connectivity of mouse somatosensory and prefrontal cortex examined with trans-synaptic tracing. Nat. Neurosci. *18*, 1687–1697.

Ferezou, I., Haiss, F., Gentet, L.J., Aronoff, R., Weber, B., and Petersen, C.C.H. (2007). Spatiotemporal dynamics of cortical sensorimotor integration in behaving mice. Neuron *56*, 907–923.

Gentet, L.J., Avermann, M., Matyas, F., Staiger, J.F., and Petersen, C.C.H. (2010). Membrane potential dynamics of GABAergic neurons in the barrel cortex of behaving mice. Neuron *65*, 422–435.

Han, F., Caporale, N., and Dan, Y. (2008). Reverberation of recent visual experience in spontaneous cortical waves. Neuron *60*, 321–327.

Harris, K.D., and Thiele, A. (2011). Cortical state and attention. Nat. Rev. Neurosci. *12*, 509–523.

Jouhanneau, J.-S., Ferrarese, L., Estebanez, L., Audette, N.J., Brecht, M., Barth, A.L., and Poulet, J.F.A. (2014). Cortical fosGFP expression reveals broad receptive field excitatory neurons targeted by POm. Neuron *84*, 1065–1078.

Jouhanneau, J.-S., Kremkow, J., Dorrn, A.L., and Poulet, J.F.A. (2015). In vivo monosynaptic excitatory transmission between layer 2 cortical pyramidal neurons. Cell Rep. *13*, 2098–2106.

Lefort, S., Tomm, C., Floyd Sarria, J.-C., and Petersen, C.C.H. (2009). The excitatory neuronal network of the C2 barrel column in mouse primary somatosensory cortex. Neuron *61*, 301–316.

Luczak, A., Barthó, P., Marguet, S.L., Buzsáki, G., and Harris, K.D. (2007). Sequential structure of neocortical spontaneous activity in vivo. Proc. Natl. Acad. Sci. USA *104*, 347–352.

Manns, I.D., Sakmann, B., and Brecht, M. (2004). Sub- and suprathreshold receptive field properties of pyramidal neurones in layers 5A and 5B of rat somatosensory barrel cortex. J. Physiol. *556*, 601–622.

Mason, A., and Larkman, A. (1990). Correlations between morphology and electrophysiology of pyramidal neurons in slices of rat visual cortex. II. Electrophysiology. J. Neurosci. *10*, 1415–1428.

McGinley, M.J., David, S.V., and McCormick, D.A. (2015). Cortical Membrane Potential Signature of Optimal States for Sensory Signal Detection. Neuron *87*, 179–192.

Milenkovic, N., Zhao, W.-J., Walcher, J., Albert, T., Siemens, J., Lewin, G.R., and Poulet, J.F.A. (2014). A somatosensory circuit for cooling perception in mice. Nat. Neurosci. *17*, 1560–1566.

Moore, C.I., and Nelson, S.B. (1998). Spatio-temporal subthreshold receptive fields in the vibrissa representation of rat primary somatosensory cortex. J. Neurophysiol. *80*, 2882–2892.

Niell, C.M., and Stryker, M.P. (2010). Modulation of visual responses by behavioral state in mouse visual cortex. Neuron *65*, 472–479.

O'Connor, D.H., Peron, S.P., Huber, D., and Svoboda, K. (2010). Neural activity in barrel cortex underlying vibrissa-based object localization in mice. Neuron *67*, 1048–1061.

Okun, M., Naim, A., and Lampl, I. (2010). The subthreshold relation between cortical local field potential and neuronal firing unveiled by intracellular recordings in awake rats. J. Neurosci. *30*, 4440–4448.

Olsen, S.R., Bortone, D.S., Adesnik, H., and Scanziani, M. (2012). Gain control by layer six in cortical circuits of vision. Nature *483*, 47–52.

Otazu, G.H., Tai, L.-H., Yang, Y., and Zador, A.M. (2009). Engaging in an auditory task suppresses responses in auditory cortex. Nat. Neurosci. *12*, 646–654.

Pinto, L., Goard, M.J., Estandian, D., Xu, M., Kwan, A.C., Lee, S.-H., Harrison, T.C., Feng, G., and Dan, Y. (2013). Fast modulation of visual perception by basal forebrain cholinergic neurons. Nat. Neurosci. *16*, 1857–1863.

Polack, P.-O., Friedman, J., and Golshani, P. (2013). Cellular mechanisms of brain state-dependent gain modulation in visual cortex. Nat. Neurosci. *16*, 1331–1339.

Poulet, J.F.A., and Petersen, C.C.H. (2008). Internal brain state regulates membrane potential synchrony in barrel cortex of behaving mice. Nature *454*, 881–885.

Poulet, J.F.A., Fernandez, L.M.J., Crochet, S., and Petersen, C.C.H. (2012). Thalamic control of cortical states. Nat. Neurosci. *15*, 370–372.

Reimer, J., Froudarakis, E., Cadwell, C.R., Yatsenko, D., Denfield, G.H., and Tolias, A.S. (2014). Pupil fluctuations track fast switching of cortical states during quiet wakefulness. Neuron *84*, 355–362.

Sachidhanandam, S., Sreenivasan, V., Kyriakatos, A., Kremer, Y., and Petersen, C.C.H. (2013). Membrane potential correlates of sensory perception in mouse barrel cortex. Nat. Neurosci. *16*, 1671–1677.

Sakata, S., and Harris, K.D. (2009). Laminar structure of spontaneous and sensory-evoked population activity in auditory cortex. Neuron *64*, 404–418.

Sakata, S., and Harris, K.D. (2012). Laminar-dependent effects of cortical state on auditory cortical spontaneous activity. Front. Neural Circuits *6*, 109.

Sanchez-Vives, M.V., and McCormick, D.A. (2000). Cellular and network mechanisms of rhythmic recurrent activity in neocortex. Nat. Neurosci. *3*, 1027–1034.

Schiemann, J., Puggioni, P., Dacre, J., Pelko, M., Domanski, A., van Rossum, M.C.W., and Duguid, I. (2015). Cellular mechanisms underlying behavioral state-dependent bidirectional modulation of motor cortex output. Cell Rep. *11*, 1319–1330.

Schneider, D.M., Nelson, A., and Mooney, R. (2014). A synaptic and circuit basis for corollary discharge in the auditory cortex. Nature *513*, 189–194.

Vinck, M., Batista-Brito, R., Knoblich, U., and Cardin, J.A. (2015). Arousal and locomotion make distinct contributions to cortical activity patterns and visual encoding. Neuron *86*, 740–754.

Waters, R.S., Li, C.X., and McCandlish, C.A. (1995). Relationship between the organization of the forepaw barrel subfield and the representation of the forepaw in layer IV of rat somatosensory cortex. Exp. Brain Res. *103*, 183–197.

Zagha, E., Ge, X., and McCormick, D.A. (2015). Competing neural ensembles in motor cortex gate goal-directed motor output. Neuron *88*, 565–577.

Zhou, M., Liang, F., Xiong, X.R., Li, L., Li, H., Xiao, Z., Tao, H.W., and Zhang, L.I. (2014). Scaling down of balanced excitation and inhibition by active behavioral states in auditory cortex. Nat. Neurosci. *17*, 841–850.

Cell Reports, Volume *15*

Supplemental Information

Translaminar Cortical Membrane Potential Synchrony in Behaving Mice

Wen-Jie Zhao, Jens Kremkow, and James F.A. Poulet

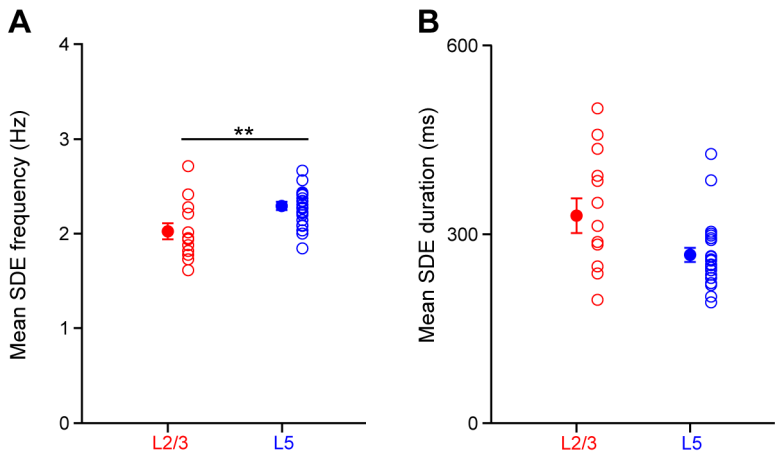

Figure S1, related to Figure 2. Characterization of slow depolarizing events during quiet wakefulness.

(A) Mean frequency of slow depolarizing events (SDE) during quiet wakefulness in L2/3 and L5 neurons. Filled circles with error bars show mean ± SEM. Open circles show individual cells.
(B) Mean duration of SDE's in L2/3 and L5 neurons.

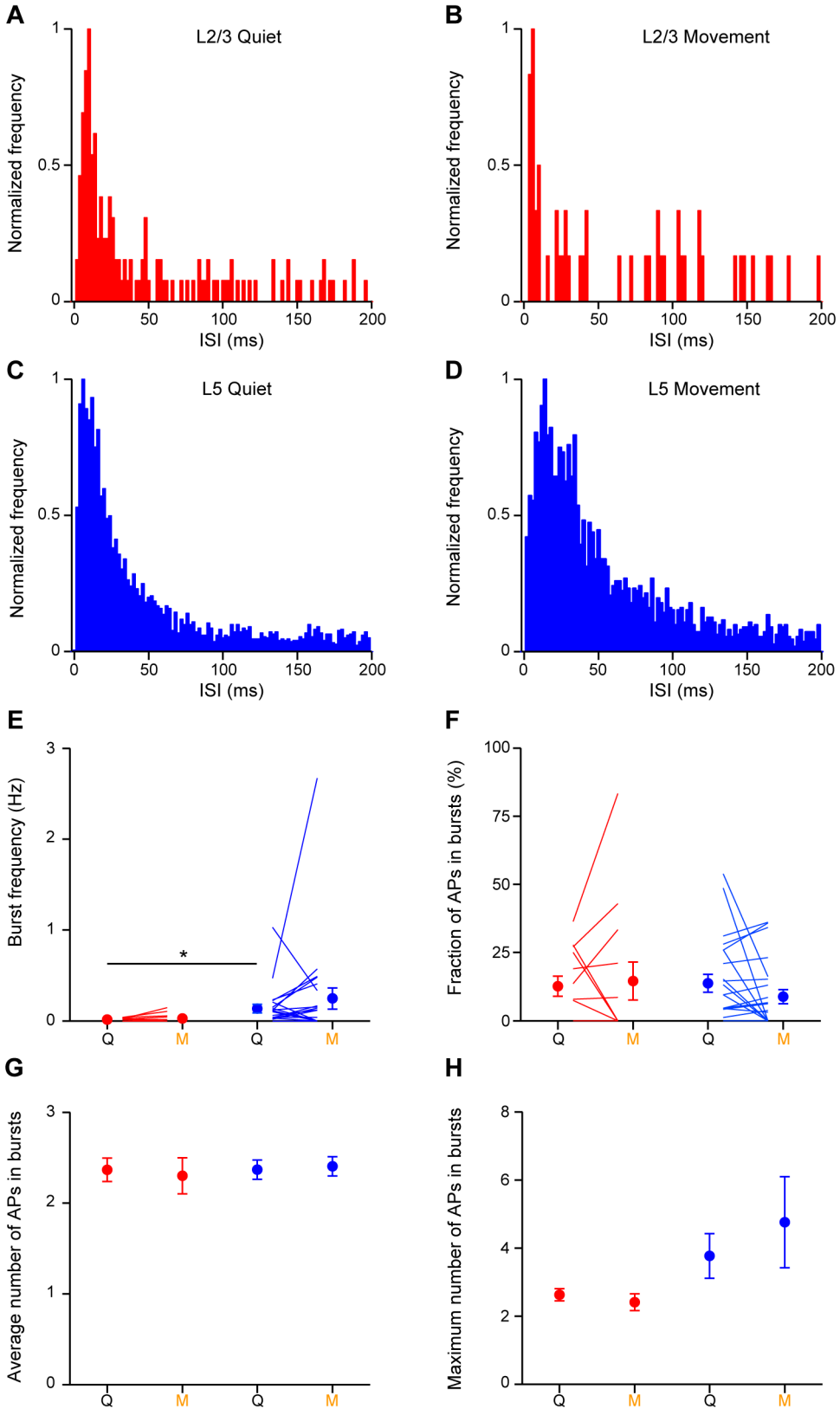

Figure S2, related to Figure 2. Analysis of spontaneous action potential bursting during quiet and moving periods

(A) Inter-spike interval (ISI) distribution of L2/3 neurons during quiet periods.
(B) ISI distribution of L2/3 neurons during moving periods.

(C) Same as (A) but for L5 neurons.
(D) Same as (B) but for L5 neurons.
(E) AP burst frequency in L2/3 and L5 during quiet and moving periods. Filled circles with error bars show mean ± SEM. Lines show individual cells. See methods for burst classification.
(F) Fraction of APs in bursts in L2/3 and L5 during quiet and moving periods.
(G) Mean number of APs in a burst is similar in L2/3 and L5 neurons. Filled circles with error bars show mean ± SEM.
(H) Maximum number of APs in a burst in L2/3 and L5 neurons.

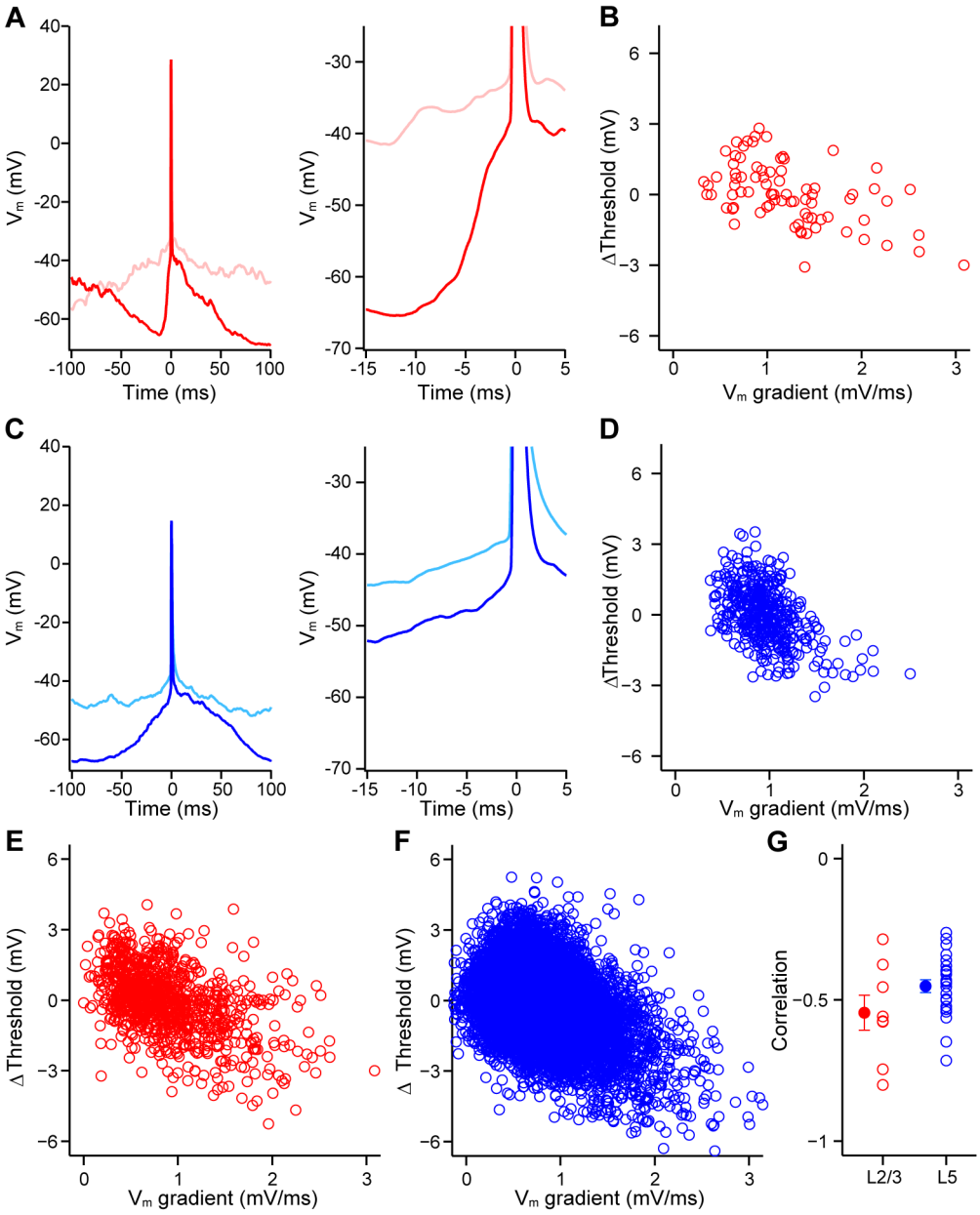

Figure S3, related to Figure 2. Action potential threshold is dependent on the speed of pre-spike depolarization in L2/3 and L5.

(A) Left: two superimposed example action potentials from a L2/3 neuron with different pre-spike V_m rise times. Right: higher temporal resolution image of the example action potentials highlights the dependence of threshold on the pre-spike V_m rise time, with a faster pre-spike depolarization resulting in a lower threshold.
(B) The difference in single spike action potential threshold from the mean action potential threshold, as a function of the gradient of the V_m in the 5 ms before action potential threshold for the example neuron in (A).
(C) Same as (A) but for a L5 neuron.
(D) Same as (B) but for the L5 neuron shown in (C).
(E) Same as (B) but for entire population of L2/3 APs.

(F) Same as (D) but for entire population of L5 APs.
(G) Pearson r correlation coefficient of the change in AP threshold versus the pre-spike V_m gradient, open circles represent individual neurons (L2/3 red, L5 blue).

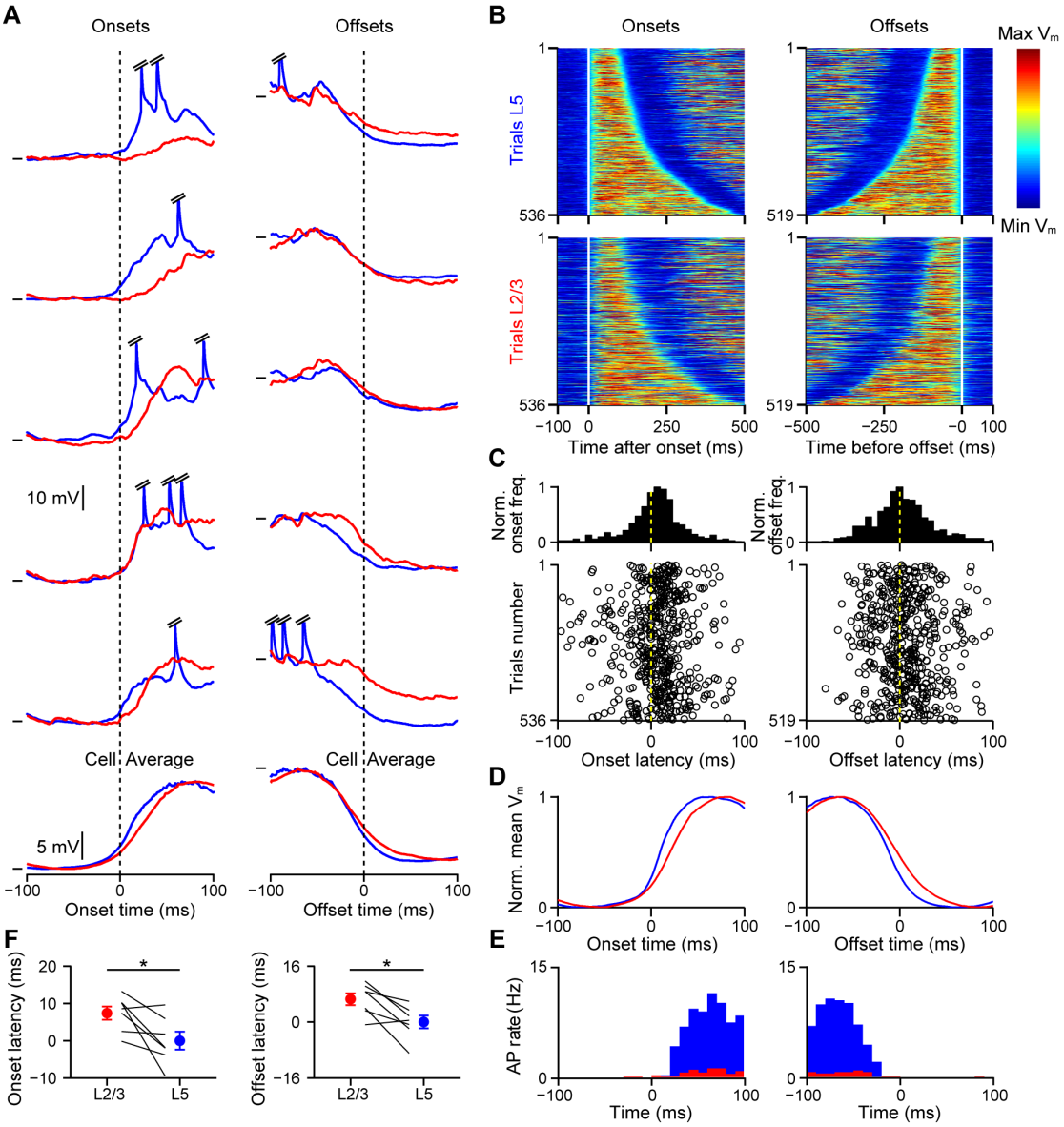

Figure S4, related to Figure 4. L5 triggered slow depolarizing events during quiet wakefulness.

(A) Example SDEs from a dual L2/3 (red) and L5 (blue) whole-cell recording in an awake, resting mouse. V_m traces are aligned to the threshold crossing at onset (left) and offset (right) of the SDE in the L5 neuron, bottom traces show V_m averages. Horizontal lines indicate for L2/3 and L5: trial 1 onset –58.9 / –57.4 mV and offset –44.6 / –39.8 mV; trial 2 onset –59.7 / –57 mV and offset –44.3 / –38.5 mV; trial 3 onset –60.5 / –53.0 mV and offset –48.9 / –44.3 mV; trial 4 onset –58.4 / –47.9 mV and offset –35.2 / –31.2 mV; trial 5 onset –56.7 / –48.4 mV and offset –42.5 / –30.9 mV. Average onset –59.7 / –53.1 mV and offset –43.0 / –37.3 mV. APs have been truncated.
(B) Plots of selected SDEs from 7 dual whole-cell recordings. SDEs were aligned at threshold crossing at the onset (left) and offset (right) of the SDE in the L5 neuron and arranged by duration. Upper boxes show L5 data and lower show L2/3 with colors corresponding to the normalized V_m from minimum (blue) to maximum (red) values.

(C) Population distribution (top) and trial-by-trial measurements (bottom) of the subthreshold onset (left) and offset (right) times in L2/3 neurons relative to the onset and offset times in L5 respectively (n = 7 dual recordings). Onset and offset times were estimated by the 5% level of a sigmoidal fit to the V_m at onset and offset (see Supplemental Experimental Procedures for details).
(D) Population average of the normalized V_m SDEs in L2/3 and L5 relative to the threshold-crossing at onset and offset of the L5 neuron.
(E) Population peri-SDE time histogram of AP times from the dataset in (D).
(F) Population analysis of onset and offset times triggered on the L5 SDE shows significantly earlier onset and offset times in L5. To calculate the onset/offset timing difference, we first measured the time of SDE onset/offset relative to the time of threshold crossing of the L5 SDE. Then we subtracted the population mean L5 onset/offset time from all values. Filled circles with error bars show mean ± SEM, lines show data from individual pairs. For all panels *$p < 0.05$, **$p < 0.01$, ***$p < 0.001$.

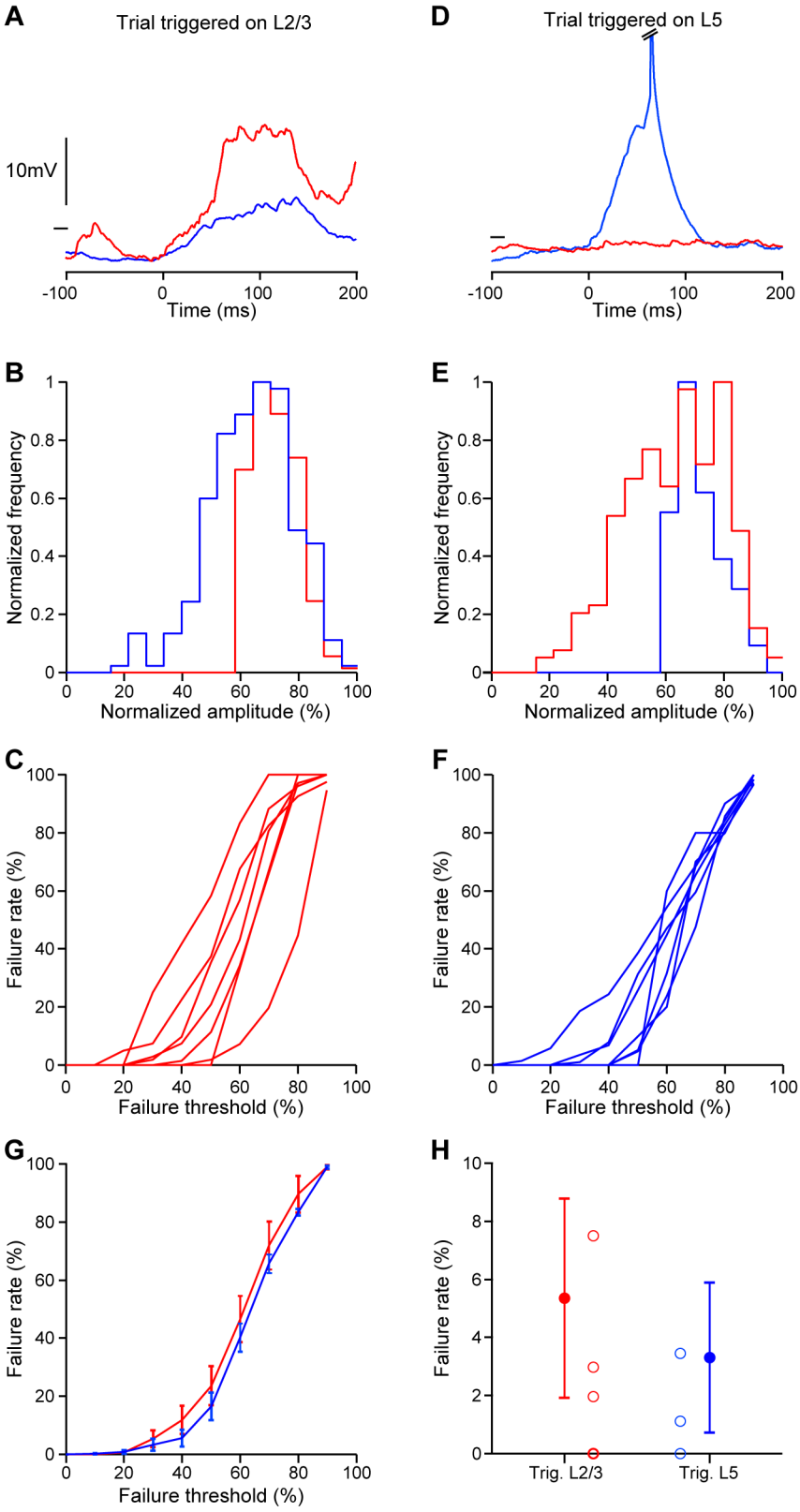

Figure S5, related to Figure 4. Small amplitude slow depolarizing events show occasional failure in other recorded layer.

(A) Example SDE from a dual recording triggered on the L2/3 activity (red) showing low amplitude event in L5 (blue), tick mark shows L5 / L2/3: –60 mV / –65 mV.
(B) Distribution of normalized SDE amplitudes when triggered on L2/3 SDEs larger than 60% of the normalized peak amplitude (see Supplemental Experimental Procedures).
(C) Failure rate as a function of failure threshold when triggering on L2/3. Failure threshold was the SDE amplitude in L5 below which a SDE was counted as a failure.
(D) Same as (A) but triggered on a L5 SDE, tick mark shows L5/L2/3: –60 mV / –68 mV.
(E) Same as (B) but triggered on a L5 SDE.
(F) Same as in (C) but triggered on a L5 SDE. Failure threshold was the SDE amplitude in L2/3 below which a SDE was counted as a failure.
(G) Population averaged failure rates when triggered on L2/3 (red) and L5 (blue).
(H) Failure rates when triggering on different layers at a failure threshold of 30% amplitude.

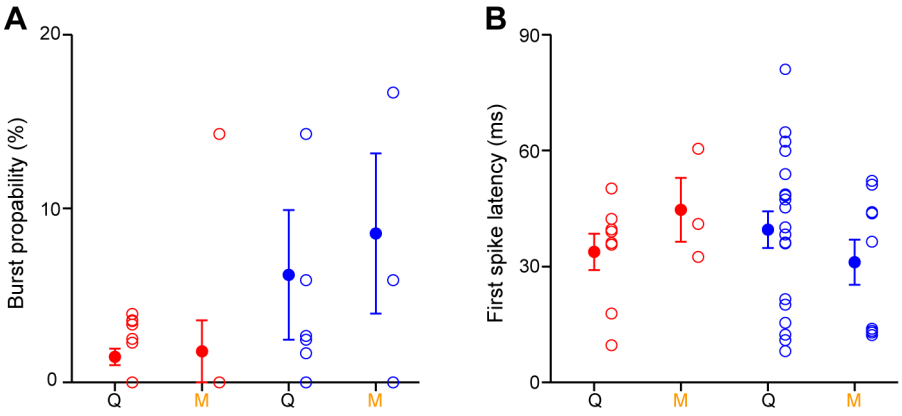

Figure S6, related to Figure 6. Sensory-evoked action potential bursting.

(A) Action potential burst probability during the sensory response in L2/3 and L5 neurons during quiet and moving periods. Burst probability was calculated as the fraction of trials in which a burst was detected in the 100 ms following stimulus onset. Filled circles with error bars show mean ± SEM. Open circles show individual cells.
(B) Sensory-evoked first spike latency was similar in L2/3 and L5 during quiet and moving periods.

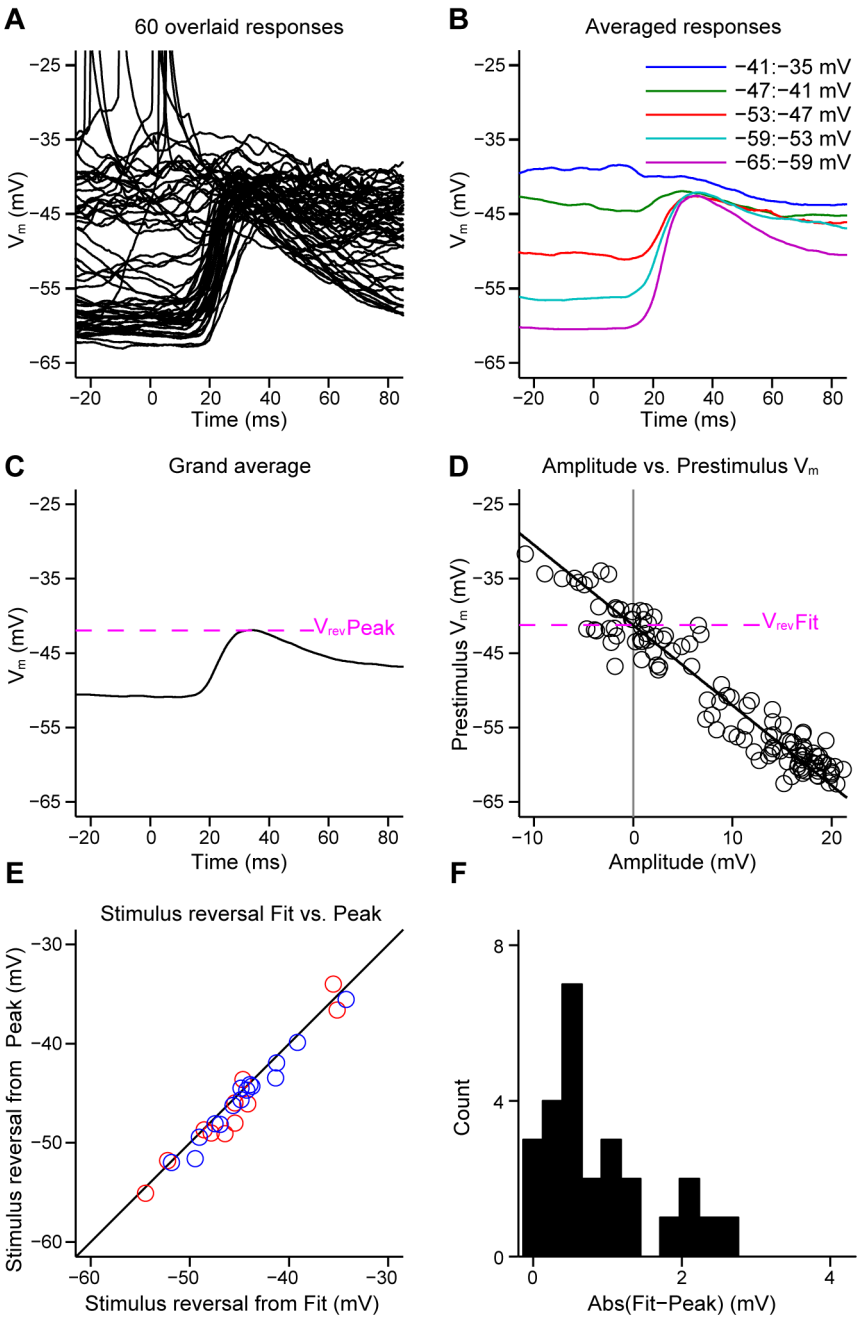

Figure S7, related to Figure 6. Measurement of the tactile stimulus-evoked reversal potential.

(A) Example trial-by-trial V_m responses of a L2/3 cortical neuron to tactile stimulation of the forepaw digits in an awake mouse.
(B) Averaged tactile-evoked responses from neuron in (A) grouped into 5 categories based on the pre-stimulus V_m show a reduced response amplitude at more depolarized V_m values.
(C) Grand average from the example neuron in (A and B), pink dashed line shows the peak V_m of the grand average response ($Vrev_{Peak}$).
(D) Plot of the amplitude of all individual tactile-evoked responses (open circles) from example neuron in (A to C) against the pre-stimulus V_m. Pink

dashed line shows the reversal potential as defined by the point at which the linear fit (black line) crosses the 0 mV tactile-stimulus evoked response amplitude (grey line).
(E) The peak V_m of the average tactile-evoked response (as in C) plotted against the reversal potential as determined by fitting the individual responses (as in D) shows significant correlation across all recorded cells. Red circles show L2/3 cells and blue circles L5 cells.
(F) Distribution of the differences in reversal potential as measured by both methods. The mean distance was 1.00 ± 0.15 mV.

SUPPLEMENTAL EXPERIMENTAL PROCEDURES

Surgery and intrinsic optical imaging

Male 6 to 9 week old C57bl6J mice were anesthetized with isoflurane (1.5 to 2% in O_2) and implanted with a lightweight metal head support. The skull was exposed over forepaw S1 and a recording chamber made from dental cement (Paladure, Heraeus Kulzer). The forepaw representation of digit 3 (D3) was identified with intrinsic optical imaging. D3 was stimulated with a piezo-element at 10 Hz during red light illumination of the skull. The intrinsic optical signal and blood vessel patterns were then used to guide the location of the craniotomies. On the day of the experiment, mice were anesthetized and for single recording experiments, one craniotomy was made over the center of the D3 intrinsic signal. For dual recordings, two < 0.5 mm diameter craniotomies were drilled next to each other, one directly over the center of the D3 intrinsic signal response and the second more lateral to attempt to target L5 and L2/3 neurons in the same column. The exposed brain was covered with Kwik-Cast (WPI) and mice were allowed to recover for > 3 hours following surgery before attempting whole-cell recordings.

Monitoring forepaw movement and tactile stimulation

Mice were habituated to head-fixation over 3 days. The right forepaw was tethered to the recording platform with digits 2, 3 and 4 overhanging the platform edge. A force-feedback movement sensor arm (Aurora Scientific, Dual-Mode Lever Arm Systems 300-C) was positioned underneath digit 3. The sensor arm was held in contact with the glabrous skin of digit 3 with constant force throughout the recordings and provided an online monitor of digit movement as well as delivery of tactile stimuli. Brief (2 ms) tactile stimuli were delivered at a pseudo-randomized time interval (between 2 s and 4 s). Paw movement and sensory stimulation were recorded and delivered alongside neuronal recordings at 20 kHz via an ITC18 board (Heka) under the command of IGOR Pro (Wavemetrics) software.

Electrophysiological recordings

Whole-cell recordings were made with 2 mm external diameter borosilicate glass pipettes (Hilgenberg) with a resistance of 5-7 MΩ. Pipettes were filled with intracellular recording solution, in mM: 135 K-gluconate, 4 KCl, 10 HEPES, 10 Na_2phosphocreatine, 4 MgATP, 0.3 Na_3GTP (adjusted to pH 7.3 with KOH), 2 mg/ml biocytin (Sigma). The brain was covered with Ringer's solution containing, in mM: 135 NaCl, 5 KCl, 5 HEPES, 1.8 $CaCl_2$, 1 $MgCl_2$. An Ag/AgCl ground electrode was placed in the recording chamber. Blind whole-cell recordings were then targeted to L2/3 (subpial depth 100 to 400 µm) and/or L5 (subpial depth 600 to 1000 µm) and performed with a Multiclamp 700b (Molecular Devices) amplifier in current clamp mode at 20 kHz via an ITC18 A/D board and filtered between 0 and 10 kHz. During dual recordings, pipettes were inserted into separate, neighboring craniotomies. The L2/3 pipette was inserted into the D3 craniotomy normal to cortical surface, while the second pipette was inserted through the second, more lateral craniotomy at 45 degrees from vertical to target L5. The recording depths reported in Figure 1 that were not identified with biocytin staining were calculated by triangulation using the angle of the pipette and distance from the pial surface measured by the micromanipulator reading. Intrinsic membrane properties were measured with current injection performed soon after break-in. The V_m was not corrected for the liquid junction potential.

Histological processing

Mice were transcardially perfused with 4% paraformaldehyde (PFA) under deep urethane anesthesia (2.5 g per kg of body weight). The brains were fixed in 4% PFA for at least 12 hours and then placed in phosphate buffer until further processing. 100 µm coronal slices were made using a Leica VT1000 S vibrating microtome. Next, slices were stained for cytochrome oxidase and then for biocytin using an ABC kit (Vectastain). Stained slices were mounted in Moviol and stored in the fridge at 4°C. Neurolucida (MicroBrightField) software was used to reconstruct and photograph stained neurons.

Data analysis

Data were analyzed using custom written scripts in IGORpro (Wavemetrics) and Matlab (MathWorks). All data were statistically analyzed using non-parametric tests, paired data with a Wilcoxon signed rank test and unpaired data with a Wilcoxon rank sum test. Statistical tests are within the same layer across different states (e.g. L2/3 Q versus L2/3 M or L5 QQ versus L5 QM) and across layers within the same state (e.g. L2/3 Q versus L5 Q) but not across layers in different states (e.g. L2/3 Q versus L5 M).

Input resistance

–100 pA, 100 ms current pulses were used to test for input resistance soon after break-in. The change in V_m due to access resistance during input resistance measurements was subtracted from the V_m off-line (Crochet and Petersen, 2006). Access resistance was calculated using an exponential fit of the V_m from a 2 ms period after the start of current injection. The difference in V_m between the baseline and the time point at which the fit crossed the onset time of current injection was taken as the access resistance.

After-hyperpolarization

The after-hyperpolarization (AHP) was calculated as the difference between the baseline V_m at 150 to 50 ms before current injection and the most negative peak in the 100 ms after current injection. The baseline was measured as the mean V_m throughout baseline period, the peak was measured as the mean V_m ± 0.5 ms around the peak AHP.

Behavioral state classification

Moving and quiet periods were selected based on the digit movement signal ($digit_{mov}$). Movement onsets and offsets were detected by thresholding the rectified first derivative ($digit_{FD}$) of the digit movement signal (the $digit_{mov}$ was smoothed using a moving average with a 50 ms window before calculating the first derivative). We used a low threshold (~0.5–2 SD) to reliably detect even small/short movements. In some cases this low threshold resulted in the detection of multiple movement onsets/offsets during long digit movements. To extract only one movement onset and offset in these cases we combined

all onsets/offsets that were less than 500 ms apart and kept only the first onset and last offset. Using these detected movement onsets/offsets we then split the data into quiet and moving epochs of 2 to 4 s duration (see below). To have a clean separation between quiet and moving states we excluded quiet periods that were followed or preceded by a moving state by less than 1 s.

Resting/moving analysis

The detected quiet and moving periods were split into 2 s long epochs to characterize the V_m properties (mean, SD, correlation etc.) shown in Figures 2 and 3. The mean number of epochs/cell was 110.51 ± 10.84 for quiet epochs and 19.45 ± 2.26 for moving epochs. We detected AP thresholds by peaks in the third derivative of the V_m and removed APs from the V_m when analyzing the subthreshold characteristics of the V_m. To characterize the frequency spectrum of the V_m we calculated the fast Fourier transform (FFT) of the baseline subtracted V_m using the FFT function in Matlab. The power of the FFT at low frequencies was measured as the area under the FFT between 1–5 Hz. Cross correlation analysis between pairs of cells was made after the V_m had been baseline subtracted and normalized by the SD. The coherence between pairs of cells was calculated using:

$$Cxy(f) = \frac{|Sxy(f)|^2}{Sxx(f) * Syy(f)}$$

with Sxx and Syy being the power spectra of the two V_m's and Sxy the cross-spectrum. The analysis shown in Figure 2H was done for the entire dataset, i.e., without splitting the data into quiet and moving periods. Here the average V_m value of the depolarized membrane state (Max V_m) was estimated by averaging the 10% most depolarized V_m values.

Slow depolarizing events analysis

To characterize the depolarizing events during quiet periods we selected 4 s long quiet epochs. To detect the onsets and offsets of the depolarizing events (Figure 4A) we smoothed the V_m (25 ms moving average), and thresholded the smoothed V_m at 25–30% of the distance (V_m range) between the Min V_m (the V_m value of the hyperpolarized membrane state) and the Max V_m (the V_m

value of the depolarized membrane state). Min/Max V_m were calculated from the mean 5% of the most hyperpolarized/depolarized V_m values. We included only events with a duration > 100 ms and an average V_m between onset and offset larger than 60% of the V_m amplitude. Furthermore, we excluded events that were preceded by another depolarizing event by less than 100 ms. To calculate the grand average of the onsets/offsets of the depolarizing events we aligned all events to threshold crossing. To estimate the latency between the L2/3 and L5 cell pair at the onset/offset of depolarizing events we fitted each V_m around the onset/offset (± 100 ms) with a sigmoidal function. The latency was then estimated from the time difference at the 5% level of the sigmoidal fits. We included only onsets/offsets in which the fits of both L2/3 and L5 had a goodness-of-fit > 0.6. To characterize the average frequency and duration of slow depolarizing events (Figure S1) we thresholded the V_m as described above. We then merged threshold crossings that were less than 50 ms apart to avoid that large but transient fluctuations during slow depolarizing events were counted as separate events. The frequency of the slow depolarizing events was then given as the number of threshold crossings per second.

Spike triggered averaging

APs were aligned to their peak V_m value time point and separated into two groups: quiet and digit movement. The gradient of a linear fit of the V_m between 22 ms and 2 ms prior to the peak of AP was used to measure the change in V_m prior to a spike (Figure 3).

Spike burst analysis

To analyze whether spikes occurred in bursts we defined the start of a burst as the time when the inter-spike interval between two consecutive spikes was shorter than 10 ms and the burst ended when the inter-spike interval was longer than 15 ms.

Movement onset analysis

To analyze the neuronal responses around the start of a digit movement we detected movement onsets using the method described above. In this

analysis we included all movements, irrespective of their amplitude and duration. The latency between the $digit_{mov}$ and V_m was then estimated by the lag of the peak in the cross correlogram between the $digit_{mov}$ and V_m around the movement onset (–200 ms to 100 ms). The change in V_m variance after movement onset was estimated by calculating the variance of the V_m in a 200 ms window across trials before (–600 to –400 ms) and around the peak after movement onset (~50 to 250 ms, gray shaded areas in Figure 5E).

Tactile response analysis

The onsets of tactile stimuli were used as triggers to study tactile-evoked responses. To classify the behavioral state during tactile stimulation we calculated the amplitude/maximum of the $digit_{mov}$ in a window 300 ms before and 300 ms after stimulation. Using these two measurements we then classified each trial into three categories: quiet-quiet = no movements before and after tactile stimulation, quiet-moving = no movements before but movements after tactile stimulation, moving-moving = movements before and after stimulation. Trials with movements before but not after sensory stimulation were excluded from the analysis. No movement was defined as amplitudes < 1.5*median of all amplitudes and movements were defined as amplitudes > 2.5*median of all amplitudes.

The amplitude of tactile responses (Figures 6E and 7D) was estimated as the difference between the V_m at the stimulus onset (pre-stimulus, 0 ms) and the V_m at the peak of the response. To calculate the trial-by-trial correlation between the tactile-evoked responses of simultaneously recorded cell pairs (Figures 6J and 6K) we calculated the Pearson correlation coefficient between the response amplitudes of both cells. The latency (Figure 6I) was estimated by fitting a sigmoidal function to the average evoked response between stimulus onset and the peak of the response. The time at which the fit crossed 3% of the amplitude was used as a measure of latency.

The tactile-evoked response reversal potential (V_{rev}) was measured using two complementary methods. First, V_{rev} was estimated by linear regression of the amplitude versus the pre-stimulus V_m relationship. For this we fitted a line into the amplitude versus pre-stimulus V_m data and extracted

V_{rev} as the pre-stimulus V_m for which the amplitude was 0 from the fitted line (Figure S7D). In addition, we were able to estimate V_{rev} by the peak of the averaged tactile-evoked response (Figure S7C). This method resulted in almost exactly the same estimates of V_{rev}, as compared to the line-fitting method (Figure S7E, correlation = 0.97, p = 0, mean difference between fit and peak = 1.00 ± 0.15 mV).

The tactile-evoked spiking response (Figure 6F) was calculated by measuring the firing rates in a 100 ms window after stimulus onset (0–100 ms) and by subtracting the baseline firing rate (baseline firing rate was estimated in a 100 ms window before stimulus onset). To calculate the evoked spiking response in the late phase of the tactile response (Figure 7G) we measured the firing rate in the window between 300 and 400 ms after stimulus onset and subtracted the baseline firing rate. To show the relationship between the evoked firing rates and the distance between AP threshold and V_{rev} (Figure 6H) we measured the firing rate in the 100ms window after stimulus onset.

The average V_m during the pre-stimulus phase (Figure 7E) was calculated in a 100 ms window before stimulus onset (from –100 ms to 0 ms), and the average V_m of the late phase (Figure 7F) was calculated between 300 and 400 ms after stimulus onset.